© 2019. Published by The Company of Biologists Ltd | Development (2019) 146, dev175893. doi:10.1242/dev.175893

RESEARCH ARTICLE

Adaptive correction of craniofacial defects in pre-metamorphic *Xenopus laevis* tadpoles involves thyroid hormone-independent tissue remodeling

Kaylinnette Pinet, Manas Deolankar, Brian Leung and Kelly A. McLaughlin*

ABSTRACT

Although it is well established that some organisms can regenerate lost structures, the ability to remodel existing malformed structures has been less well studied. Therefore, in this study we examined the ability of pre-metamorphic *Xenopus laevis* tadpoles to self-correct malformed craniofacial tissues. We found that tadpoles can adaptively improve and normalize abnormal craniofacial morphology caused by numerous developmental perturbations. We then investigated the tissue-level and molecular mechanisms that mediate the self-correction of craniofacial defects in pre-metamorphic *X. laevis* tadpoles. Our studies revealed that this adaptive response involves morphological changes and the remodeling of cartilage tissue, prior to metamorphosis. RT-qPCR and RNA-seq analysis of gene expression suggests a thyroid hormone-independent endocrine signaling pathway as the potential mechanism responsible for triggering the adaptive and corrective remodeling response in these larvae that involves *mmp1* and *mmp13* upregulation. Thus, investigating how malformed craniofacial tissues are naturally corrected in *X. laevis* tadpoles has provided valuable insights into the maintenance and manipulation of craniofacial morphology in a vertebrate system. These insights may help in the development of novel therapies for developmental craniofacial anomalies in humans.

KEY WORDS: *Xenopus laevis*, Craniofacial, Morphology, Tissue remodeling, Retinoid X receptor, Prolactin

INTRODUCTION

Craniofacial abnormalities, such as cleft palate, fetal alcohol syndrome and microcephaly are seen in over 1/700 births worldwide among humans (Blanco-Davila, 2003; Gregg et al., 1994). Unfortunately, most craniofacial abnormalities affecting humans are untreatable and the few available treatment options involve expensive and invasive surgeries. Thus, research focusing not only on the causes, but also the resolution, of craniofacial defects in vertebrates has never been more crucial.

The spatiotemporally regulated pathways that coordinate cell division, migration, apoptosis and differentiation during craniofacial development are highly conserved across vertebrates (Simoes-Costa and Bronner, 2015; Square et al., 2015). These conserved gene regulatory networks are crucial for the specification and differentiation of key cell populations, such as the cranial neural crest cells: a vertebrate-specific cell population that actively migrates anteriorly during development and differentiates into several craniofacial tissues [e.g. neurons, cartilage, and connective tissue (Simões-Costa and Bronner, 2015; Simões-Costa et al., 2015)]. Environmental factors, including vitamin A levels and pH, also play a role in the specification and differentiation of cells during embryogenesis (Vandenberg et al., 2011; Yelin et al., 2007). Ultimately, the intricate processes involved in creating a head leave organisms vulnerable to the possibility of craniofacial defects during embryogenesis.

Craniofacial abnormalities that are commonly seen in humans can be recapitulated in several other vertebrates (e.g. mice, fish and frogs) through exposure to the same teratogens during development. For example, exposing *X. laevis* embryos to ethanol can cause eye and brain malformations, similar to those seen in humans with fetal alcohol syndrome (Fainsod and Kot-Leibovich, 2017; Kot-Leibovich and Fainsod, 2009; Yelin et al., 2007, 2005). The similarities among craniofacial phenotypes in vertebrates provide us with the great opportunity to use model organisms to better understand human craniofacial defects.

Although numerous studies have described various causes of craniofacial abnormalities in vertebrates, only one study has reported the natural resolution of craniofacial deformities in vertebrates. This study, carried out by Vandenberg et al., revealed that altering membrane voltage, pH and gene expression patterns in *X. laevis* embryos by knocking down H^+-V-ATPase channel function induces a wide range of craniofacial defects in tadpoles, some of which are subsequently normalized over time (Vandenberg et al., 2012). Vandenberg et al. confirmed that the normalization of craniofacial defects occurred prior to metamorphosis by using geometric morphometric analysis to quantify the changes in morphology over time. Interestingly, an unrelated study examining normal *X. laevis* craniofacial structures noted that variance in craniofacial cartilage morphology among wild-type *X. laevis* tadpoles decreases prior to metamorphosis (Rose et al., 2015). Combined, these studies suggest that *X. laevis* tadpoles possess an endogenous mechanism responsible for monitoring and adaptively adjusting craniofacial morphology, prior to metamorphosis.

Thus, we resolved to further investigate the biological mechanisms responsible for the ability of pre-metamorphic *X. laevis* tadpoles to self-correct abnormal craniofacial phenotypes. This involved qualitative and quantitative analysis of whole-head and craniofacial tissue (i.e. cartilage and eye tissue) morphology, throughout pre-metamorphic stages, in tadpoles with a variety of craniofacial abnormalities; followed by gene expression profile analysis to identify the molecular factors involved in initiating and/or carrying out the self-correction of abnormal craniofacial morphology in these animals. For this research, a set of perturbations that induced consistent abnormal head phenotypes was required;

Department of Biology, Allen Discovery Center, Tufts University, 200 Boston Ave., Suite 4700, Medford, MA 02155, USA.

*Author for correspondence (kelly.mclaughlin@tufts.edu)

K.A.M., 0000-0002-2541-2189

Received 18 January 2019; Accepted 20 June 2019

Development (2019) 146, dev175893. doi:10.1242/dev.175893

the perturbations used included three different pharmacological exposures (thioridazine, ethanol and ICI 118,551) and one morpholino-based treatment (xMLTK-MO). All of these treatments vary in their known biological effects: thioridazine is a dopamine-receptor antagonist, ICI 118,551 is a β_2 inverse agonist, ethanol is a retinol antagonist and xMLTK-MO hinders chondrogenesis (Table 1) (Suzuki et al., 2012). Despite the differences in biological activity, these perturbations all reliably produce abnormal craniofacial morphologies among early pre-metamorphic *X. laevis* tadpoles. Once uniform abnormal craniofacial structures were induced, craniofacial morphology was examined at various developmental stages to probe the ability of *X. laevis* to remodel malformed structures prior to metamorphosis.

By monitoring the craniofacial deformities induced by these four different perturbations throughout pre-metamorphic life stages, we determined that pre-metamorphic *X. laevis* tadpoles can self-correct some, but not all, craniofacial malformations. We also compared cartilage tissue morphology and gene expression profiles between wild-type tadpoles, tadpoles with correctable craniofacial abnormalities and tadpoles with seemingly permanent craniofacial defects. Using this approach, we found that the improvement of overall craniofacial morphology in tadpoles with correctable craniofacial abnormalities is largely due to the remodeling of cartilage and eye tissue. Furthermore, this adaptive tissue remodeling is independent of thyroid hormone signaling, may depend on prolactin hormone signaling, and involves the upregulation of *mmp1* and *mmp13*.

RESULTS

Craniofacial defects caused by xMLTK-MO, thioridazine and ethanol (but not ICI 118,551) improve in pre-metamorphic tadpoles

To examine the potential of tadpoles to self-correct malformed structures, several treatments were used to induce abnormal anterior structures. For example, to reproducibly alter craniofacial morphology (cartilage reduction and smaller eyes), we used a morpholino that has previously been shown to hinder chondrogenesis (xMLTK-MO) by Suzuki et al. (Suzuki et al., 2012) (Fig. 1A, Fig. S1). Additional reproducible craniofacial defects were attained through the temporally regulated exposure of neurula stage embryos to thioridazine, ethanol or ICI 118,551 (Fig. 1, Fig. S1). We found that all three of the pharmacological perturbations altered the expression pattern of the cranial neural crest marker *sox9* in tailbud-stage *X. laevis* (Fig. S2A,B), which suggests that these treatments do not prevent the specification of cranial neural crest cells; instead, they may hinder CNCC migration, differentiation or proliferation. Although xMLTK-MO does not perturb *sox9* spatiotemporal expression in developing *X. laevis*, it hinders chondrogenesis by preventing the upregulation of a chondrogenic transcription factor gene, *sox6*, by Sox9 (Suzuki et al., 2012).

Table 1. Biological function of genetic and pharmacological perturbations used in this study

Perturbation	Biological activity	Reference(s)
xMLTK morpholino	Inhibitor of Sox6 transcription	Suzuki et al. (2012)
Thioridazine	Dopamine receptor antagonist	Kilts et al. (1984)
ICI 118,551	Selective β_2 inverse agonist	Bylund et al. (1994); Skeberdis et al. (1997)
Ethanol	Retinol antagonist	Kot-Leibovich and Fainsod (2009); Marrs et al. (2010); Yelin et al. (2007)

Each of the pharmacological treatment groups displayed abnormal craniofacial phenotypes. Finite thioridazine exposure during neurulation results in an abnormally rectangular head morphology, as opposed to the more-rounded overall head morphology of stage-matched controls (Fig. 1A). This rectangular head phenotype emerges from the decreased branchial arch size (Fig. 1A) and malformed mouth (Fig. 1B) of the thioridazine-treated tadpole, characteristics that were seen in virtually all specimens exposed to thioridazine (Fig. S1). In addition to the rectangular head phenotype, thioridazine-treated tadpoles frequently have misshaped eyes (Fig. 1A). Similarly, the ICI 118,551-exposed embryos developed into tadpoles with a more-trapezoidal head phenotype, due to a drastically underdeveloped mouth region and reduction in overall head size (Fig. 1A,B). The ethanol exposure (which was also restricted to NF stages 13-26) consistently produced viable tadpoles with reduced overall head size, occasionally with misshaped eyes (Fig. 1A).

Once facial defects had been induced, geometric morphometric analysis was used to quantify the changes to and resolution of malformed or mispositioned craniofacial features (e.g. eyes, nostrils and mouth) throughout pre-metamorphic stages. Focusing on the shape of the eye and relative angles between the midline and the nostrils or mouth edges allowed us to efficiently compare morphology across control and experimental groups, without having to adjust for differences in eye or head size (Fig. 2). Ultimately, this size-independent morphological analysis allowed us to track and investigate significant differences in allometric growth (changes in shape), as opposed to isometric growth.

Following this approach, eye shape was evaluated based on the ratio between the anterior-posterior and lateral axes of each eye. With this measure, we found that ethanol-, thioridazine- and xMLTK-MO-treated tadpoles showed a significant difference in the mean shape of their eye(s) relative to wild-type controls at NF stage 45 (Mann Whitney U-test, $P<0.001$) (Fig. 2A). Specifically, the eyes of the experimental tadpoles tended to have elongated lateral axes at NF stage 45, correlating with their abnormal eye tissue expansion towards the midline (Figs 1A and 2). The difference between control and experimental groups continuously decreased as the tadpoles progressed to NF stage 49. All three experimental groups clearly demonstrated a large improvement in eye shape between NF stages 45 and 49. In fact, when it came to the mean left eye ratios, the xMLTK-MO-treated group was no longer statistically distinguishable from controls at NF stage 49 (Fig. 2A). We must, however, note that although the xMLTK-MO-treated group showed improvement in abnormal eye shapes, the size of the affected left eye remained smaller than the control right eye (Fig. 1A).

At NF stage 49, the thioridazine-treated group showed the greatest improvement in eye shape (Fig. 2A,B). The mean difference in left and right eye ratios for these experimental tadpoles went from 0.20±0.02 (mean±s.e.m.) and 0.17±0.02 at NF stage 45, to only 0.07±0.02 (mean±s.e.m.) and 0.06±0.02 by NF stage 49. Furthermore, when we tracked the eye shape of individual tadpoles from the thioridazine experimental group, most of the experimental individuals that have abnormal eye shapes early on, match controls by stage 50 (Fig. S4). We also found that it was possible for an individual thioridazine-treated tadpole with two malformed eyes at NF stage 45 to show drastic improvement in the shape of one eye and not the other over time (Fig. 1A). Overall, we did see improvement in the abnormal eye shapes in the thioridazine, ethanol and xMLTK-MO experimental groups; however, not all the malformations were perfectly corrected by stage 50.

For the relative angles between the midline and the nostrils, the ethanol- and xMLTK-MO-treated groups did not differ from the

Development (2019) 146, dev175893. doi:10.1242/dev.175893

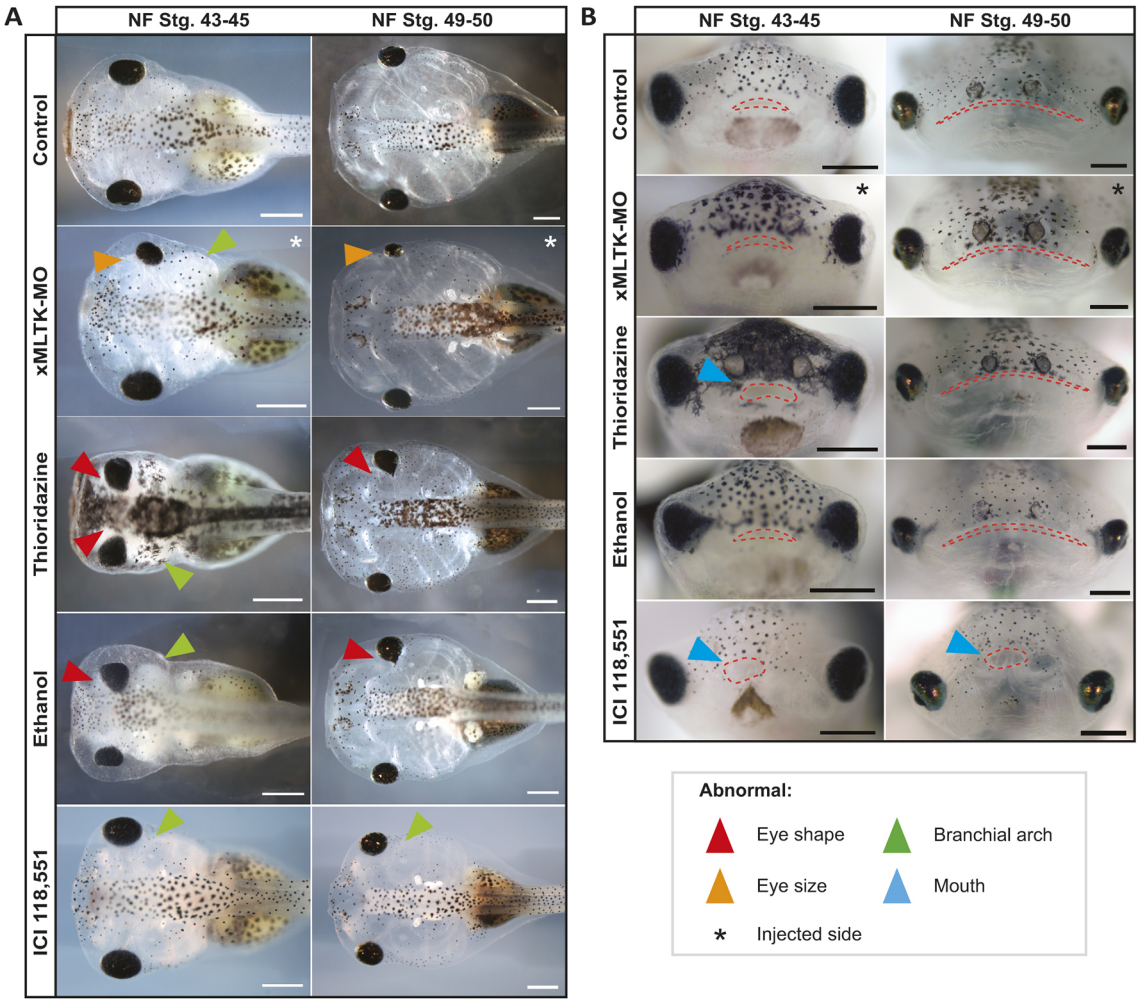

Fig. 1. Abnormal craniofacial phenotypes caused by xMLTK-MO, thioridazine and ethanol treatments can self-correct during pre-metamorphic stages. Craniofacial phenotypes of control, xMLTK-MO-, thioridazine-, ethanol- and ICI 118,551-treated tadpoles were observed at early and late pre-metamorphic stages. (A,B) Images of the same set of tadpoles at the early and late pre-metamorphic stages, dorsal (A) or anterior (B) views. xMLTK-MO, thioridazine, ethanol and ICI 118,551 treatments induce craniofacial defects that are visible by NF stages 43-45. These phenotypes improve in the case of the xMLTK-MO-, thioridazine- and ethanol-treated tadpoles by NF stages 49-50. Arrowheads indicate common craniofacial abnormalities present in treatment groups, such as abnormal eye shape, eye size, branchial arch or mouth. White asterisks indicate the injected side of xMLTK-MO tadpoles. Scale bars: 500 µm.

control values by more than 5° at any measured stage (Fig. 2C,D). At NF stage 45, the ethanol- and xMLTK-MO-treated groups have left nostril angle values that do not significantly differ from controls at NF 45 (Kruskal-Wallis U-test, $P>0.05$). Although they do show statistically significantly different nostril angles at NF stage 49 (Kruskal-Wallis U-test, $P<0.001$), it is only because the variance observed within control and experimental groups decreased as they progressed from early to late pre-metamorphic stages (Fig. 2C). The thioridazine-treated group again showed the greatest improvement with regards to the nostril-midline angle (Fig. 2C,D). The mean difference in the angle between the nostrils and midline of the thioridazine-treated tadpoles significantly differed from wild-type controls by more than 10° at NF stage 45 (Mann-Witney U-test, $P<0.001$) (Fig. 2C,D). Yet, by NF stage 49, they only differed from controls by less than 3° (Mann-Witney U-test, $P<0.01$) (Fig. 2C,D).

A slightly different pattern appeared when we measured the angle between the corner of the mouth and the midline of the experimental groups. At NF stage 45, both the left and right-side mouth measurements for the thioridazine-treated tadpoles were significantly different from controls (Mann-Witney U-test, $P<0.001$), but by NF stage 49 they had corrected so much that it was no longer statistically distinguishable from wild-type controls (Mann-Witney U-test, $P>0.05$) (Fig. 2E,F). We also saw that, on average, the xMLTK-MO-treated tadpoles showed irregular acute angles between the mouth corner and midline of their uninjected (right) side than controls at NF stage 45 (Mann-Witney U-test, $P<0.001$) (Fig. 2F). Although the right mouth corner angle in xMLTK-MO-treated tadpoles more closely matched controls by NF stage 49 (Fig. 2F), it coincided with the left mouth corner angle also becoming significantly more acute than that seen in wild-type control at that stage (Fig. 2E). Although the ethanol-treated tadpoles did not reveal significantly different mean relative mouth corner to midline angles (Fig. 2E,F), when individual ethanol-treated tadpoles were tracked, there were some that, at NF stage 46, had much more acute angles than controls, but by NF stage 50 were not differentiable from controls (Fig. S4).

Adaptive and corrective cartilage remodeling occurs between NF stage 47 and 49 in tadpoles with malformed craniofacial cartilage

Given that the chondrocranium is the main determinant of head shape in pre-metamorphic tadpoles, we investigated whether the observed changes in overall head morphology were primarily due to

Development (2019) 146, dev175893. doi:10.1242/dev.175893

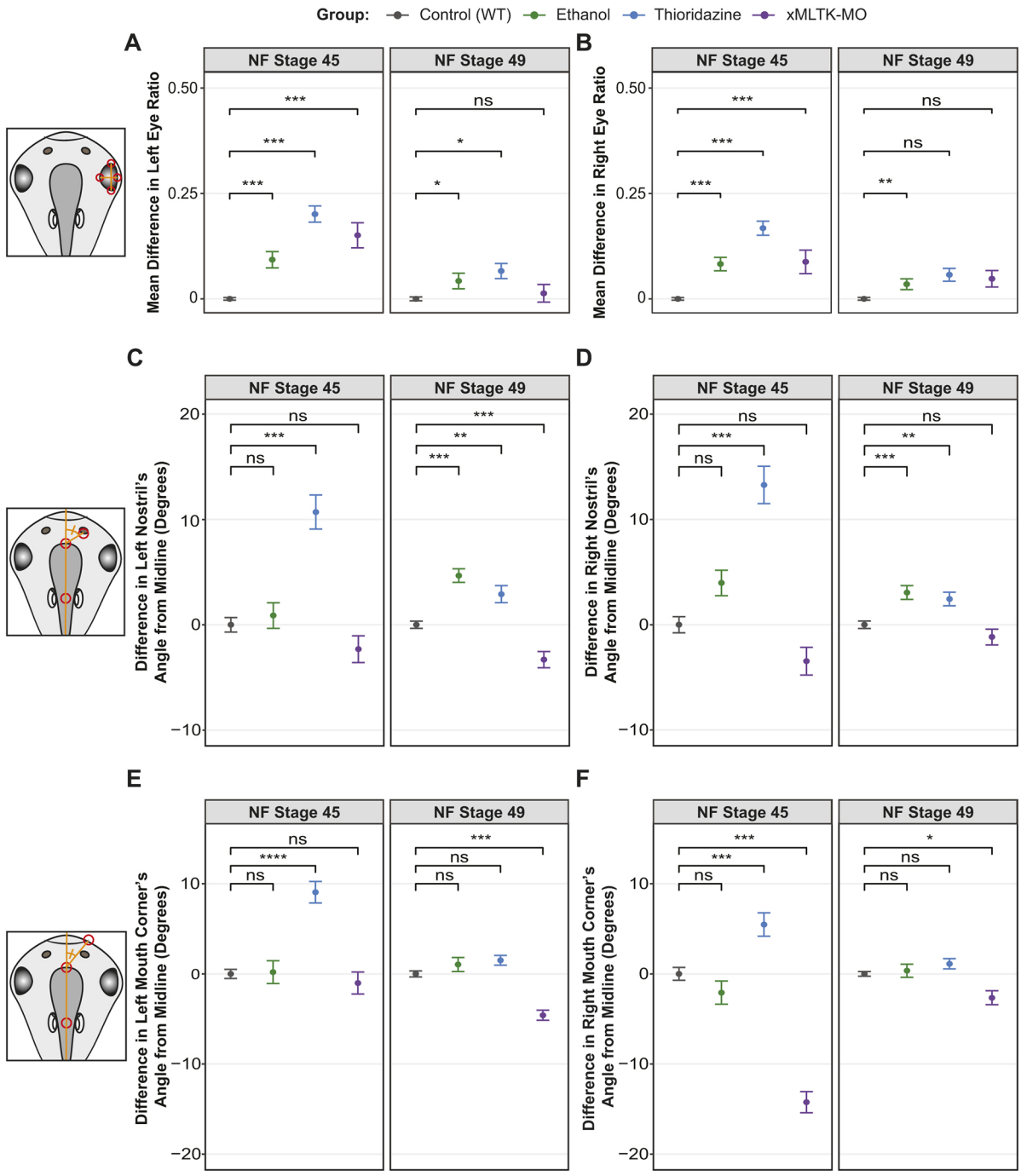

Fig. 2. Geometric morphometric analysis of corrected abnormal craniofacial morphology. Morphological metrics for (A,B) eye ratios, (C,D) nostril-midline angles and (E,F) mouth corner-midline angles were quantified for control, xMLTK-MO-, thioridazine- and ethanol-treated tadpole groups at NF stage 45 and 49. Measurements are presented as the mean difference between the experimental and control value±s.e.m. ns=P>0.05, *P<0.05, **P<0.01, ***P<0.001, ****P<0.0001 (two-tailed Mann-Witney U-test after Bonferroni adjustment); N=3-6 biological replicates, n=10-20 tadpoles per group per stage. Total n of 120 for controls, 60 for ethanol, 76 for thioridazine and 62 for xMLTK-MO.

changes in the cartilaginous scaffolding for the head. We characterized and scored changes in cartilage tissue morphology during self-correction of abnormal craniofacial at NF stages 45, 47 and 49 (Fig. 3A-C). The qualitative comparison of representative cartilage stains for control, xMLTK-MO, thioridazine, ethanol and ICI 118,551 experimental groups at NF stage 45 and 49 revealed that there is detectable improvement in the cartilage morphology of xMLTK-MO-, thioridazine- and ethanol-treated tadpoles, but not ICI 118,551-treated tadpoles (Fig. 3A,B).

With the unperturbed control group, we observed a small (3-4%) drop in the mean percentage of severe phenotypes among control tadpoles between stage 45 and 47 (Fig. 3C). However, the craniofacial cartilage scoring distribution of the control group was not significantly different at NF stages 45-47, 47-49 or 45-49 [goodness of fit (GOF) test; χ^2<4.21; d.f.=2; P>0.05] (Fig. 3C). On average, with conservative phenotype scoring (Fig. S3), no more than 10% of the control tadpoles had severely or moderately malformed craniofacial cartilage at any given stage (Fig. 3C).

Development (2019) 146, dev175893. doi:10.1242/dev.175893

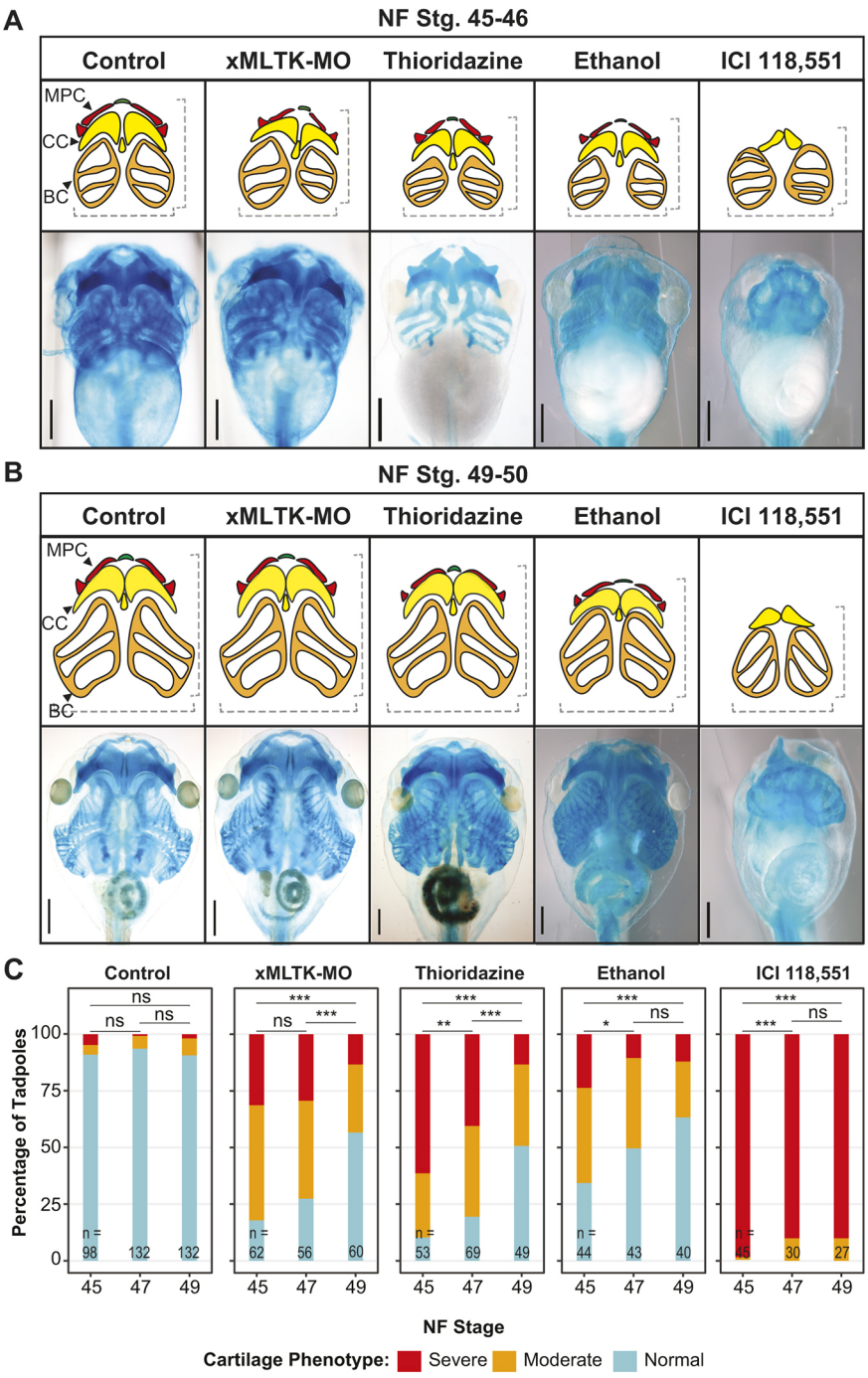

Fig. 3. Alcian Blue staining reveals corrective remodeling of cartilage in xMLTK-MO-, thioridazine- and ethanol-treated tadpoles between NF stages 45 and 50. (A,B) Representative images of bleached and Alcian Blue stained control, xMLTK-MO-, thioridazine-, ethanol- and ICI 118,551-treated specimens at NF stage 45-46 and NF stage 49-50, with corresponding cartilage schematics. MPC, Meckel's and palatoquadrate cartilage; CC, ceratohyal cartilage; BC, branchial cartilage. (C) Craniofacial cartilage phenotypes were scored as normal, moderate or severe (see Fig. S3 for scoring reference). Goodness of fit χ^2 tests for each group were performed with the expected distributions set to the mean percentage distributions of stage 45; ns=P>0.05, *=P<0.05, **=P<0.01, ***=P<0.001 after Bonferroni adjustment; N=2-4 biological replicates, n=15-33 tadpoles per group per stage; total n is shown in the graphs. Scale bars: 500 µm.

Given that xMLTK-MO specifically hinders chondrogenesis, it is not surprising that ∼80% of xMLTK-MO-injected tadpoles had noticeably malformed craniofacial cartilage at NF stage 45 (Fig. 3C). These malformations were dramatically reduced a few stages later (NF stg. 49) when only 43% of treated animals had malformed craniofacial cartilage (Fig. 3C). Although there was a significant difference between stage 45 and 49 (GOF test; χ^2=102.59; d.f.=2; P<0.001), further comparisons between NF stages 45-47 (GOF test; χ^2=6.31; d.f.=2; P>0.05) and 47-49 (GOF test; χ^2=43.89; d.f.=2; P<0.001) revealed that this was primarily due to changes between the latter pair (Fig. 3C). These data suggest that adaptive cartilage remodeling primarily occurs during and after NF stage 47 in xMLTK-MO-treated tadpoles. Thus, we have confirmed that the malformed cartilage in xMLTK-MO-treated tadpoles improves between stages 45 and 49, although the improvement seen in xMLTK-MO-treated tadpoles was not as drastic as that seen with the thioridazine-treated tadpoles.

For the thioridazine experimental group, the craniofacial cartilage scoring distribution is significantly different between all stages examined (NF stages 45-47, 47-49 and 49-50; GOF test; 196.63≥χ^2≥19.99; d.f.=2; P<0.001) (Fig. 3C). At stage 45, more than 60% of the thioridazine-treated tadpoles had severely malformed craniofacial cartilage, but only 13% were severely malformed by stage 49 (Fig. 3C). This suggests that the malformed cartilage is adaptively remodeling its shape during pre-metamorphic stages to reach a target morphology.

Development (2019) 146, dev175893. doi:10.1242/dev.175893

Even the ethanol-treated tadpoles, which possessed the mildest cartilage defects of all the experimental groups, still demonstrated a drop from 24% to only 12% severe craniofacial cartilage phenotypes between NF stages 45 and 49 (Fig. 3C). Craniofacial scoring distributions for the ethanol-treated tadpoles were significantly different between NF stage 45 and 47 cartilage (GOF test; χ^2=14.23; d.f.=2; P<0.001), but not between stages 47 and 49 (GOF test; χ^2=9.80; d.f.=2; P>0.05) (Fig. 3C). Therefore, they do not undergo cartilage remodeling under the same timeline as the xMLTK-MO- or thioridazine-treated tadpoles.

Finally, ICI 118,661 exposure had the most dramatic impact on craniofacial cartilage of all the experiment groups. At any given pre-metamorphic stage, 90-98% of the ICI 118,551-treated tadpoles had severely malformed (or missing) craniofacial cartilage (Fig. 3C). For the ICI 118,551-treated group, the craniofacial cartilage scoring distribution is significantly different between NF stages 45 and 47 (GOF test; χ^2=42.37; d.f.=2; P<0.001), but not between stages 47 and 49 (GOF test; χ^2=0; d.f.=2; P>0.05) (Fig. 3C). These data suggest that if craniofacial cartilaginous features are missing, they cannot be formed *de novo* in pre-metamorphic tadpoles, eliminating the possibility that improvement in abnormal cartilage morphology at these stages is a regenerative mechanism.

Gene expression changes during craniofacial defect remodeling do not match gene expression changes seen in tadpoles undergoing thyroid hormone-induced precocious metamorphosis

Given that *X. laevis* are known to experience major tissue remodeling during metamorphosis, we looked first towards the possible precocious involvement of thyroid hormone-dependent metamorphic pathways in the self-correction of abnormal craniofacial morphology. In wild-type tadpoles, thyroid hormone receptor α (*thrα*) and retinoid X receptor α (*rxrα*) gene expression increases at pre-metamorphic stages and their gene products form heterodimers that repress metamorphic genes, such as thyroid hormone receptor β (*thrβ*) and matrix metalloproteinase 2 (*mmp2*) (Buchholz et al., 2006; Lee and Privalsky, 2005; Li et al., 2002; Wu et al., 2001). Only when thyroid hormone begins to be produced and binds to the THRα/RXRα heterodimers, do the nuclear receptors become activators of metamorphic gene expression (Das et al., 2006; Fujimoto et al., 2007).

As with truly metamorphic *X. laevis* tadpoles, tadpoles undergoing precocious metamorphosis show an upregulation of *thrβ* and *mmp2* (Veldhoen et al., 2014). Precocious metamorphosis can be triggered in pre-metamorphic tadpoles through exogenous exposure to the more biologically active form of thyroid hormone, triiodothyronine (T3) (Kerney et al., 2012). However, these precocious metamorphic cases are often extreme in their effect on craniofacial tissue remodeling and are frequently lethal. Consequently, we exposed wild-type pre-metamorphic tadpoles from stage 45 to 50 to a very low dose of T3 to trigger a milder form of precocious metamorphosis (Fig. S5). The gene expression profiles of these +T3 specimens represent a positive control for non-lethal, premature induction of the TH pathway.

We quantified the gene expression levels (relative to wild-type controls) for *thrα*, *rxrα*, *thrβ* and *mmp2* among +T3-, xMLTK-MO-, ethanol-, thioridazine- and ICI 118,551-treated pre-metamorphic tadpoles at various pre-metamorphic stages (Fig. 4). We also looked at the expression of retinoic acid receptor α (*rarα*) (Fig. 4). RARα is a nuclear receptor that also heterodimerized with RXRα; however, it is not directly activated by thyroid hormone (Escriva et al., 2006; Lee and Privalsky, 2005). Although fold changes in *mmp2*, *rxrα* and *thrα* among the experimental groups (particularly the ethanol and xMLTK-MO groups) were found to be significantly different from each other at NF stage 45 (Kruskal-Wallis test, d.f.=4, P<0.05), none of the experimental groups demonstrated statistically significant changes relative to wild-type controls (Dunn's test, d.f.=4, P>0.05) (Fig. 4A). Similarly, at stage 47, neither the experimental groups nor the +T3-positive control group displayed significantly altered gene expression relative to wild-type controls (Kruskal-Wallis test or Dunn's test, d.f.=4, P>0.05) (Fig. 4B). However, for *rxrα* at this stage, the +T3-positive control and xMLTK-MO-treated groups had opposing effects on gene expression and were found to be significantly different from each other (Dunn's test, d.f.=4, P<0.05) (Fig. 4B). In addition, the +T3-treated group and thioridazine-treated groups demonstrated the opposite effect on *thrβ* (Dunn's test, d.f.=4, P<0.05) (Fig. 4B).

By stage 49, the +T3 tadpole group began not only to demonstrate noticeable thyroid hormone-dependent morphological differences from wild-type controls (Fig. S5), they also began to show significant differences in *mmp2* and *thrβ* expression relative to wild-type controls (Dunn's test, d.f.=4, P<0.05) (Fig. 4C). Interestingly, the ICI 118,551- and thioridazine-treated groups also showed a biologically significant threefold increase in *thrβ* expression at NF stage 49; however, this was not statistically significant (Dunn's test, d.f.=4, P>0.05) (Fig. 4C). Furthermore, by the following developmental stage, *thrβ* expression levels in both the ICI 118,551- and thioridazine-treated groups show no fold change in expression relative to wild-type controls. Meanwhile, the +T3-treated group continued to show elevated *mmp2* and *thrβ* expression (Fig. 4D).

Taken together, the discrepancies among the gene expression profiles of tadpoles with self-correcting craniofacial abnormalities and our +T3-positive control, lead us to conclude that direct activation of the TH signaling pathway by T3 is not occurring in any of the experimental groups. To further explore these observations, we examined the effects of blocking TH signaling during the craniofacial remodeling process using the anti-thyroid drug methimazole (Degitz et al., 2005; Hornung et al., 2010; Tietge et al., 2010). Inhibiting T3 synthesis in pre-metamorphic tadpoles with correctable craniofacial defects does not affect their ability to normalize, providing strong evidence that the self-correction process is not mediated via TH-dependent events (Fig. 5). Furthermore, along with craniofacial morphological changes, the low dose T3 exposure of stage 45-50 tadpoles also caused accelerated limb bud growth (Fig. S5), a phenotype that has not been observed in any of the experimental groups.

Prolactin hormone and dopamine signaling are involved in the remodeling of malformed craniofacial tissues in pre-metamorphic thioridazine-exposed tadpoles

Having ruled out the most obvious candidate tissue remodeling pathway, we decided to take a more global RNA-seq-based approach to identifying the molecular pathways involved in the self-correction of abnormal craniofacial morphology in *X. laevis* larvae. For this experiment, we used whole-head tissue samples from thioridazine-treated tadpoles with malformed craniofacial features and compared them with wild-type controls, at NF stages 45 and 47. We chose thioridazine-treated tadpoles for this experiment because they demonstrated the most consistent abnormal phenotypes and greatest adaptive morphological changes between early and late pre-metamorphic stages. Any tissue-remodeling gene candidates found to be differentially expressed in thioridazine-treated tadpole

Development (2019) 146, dev175893. doi:10.1242/dev.175893

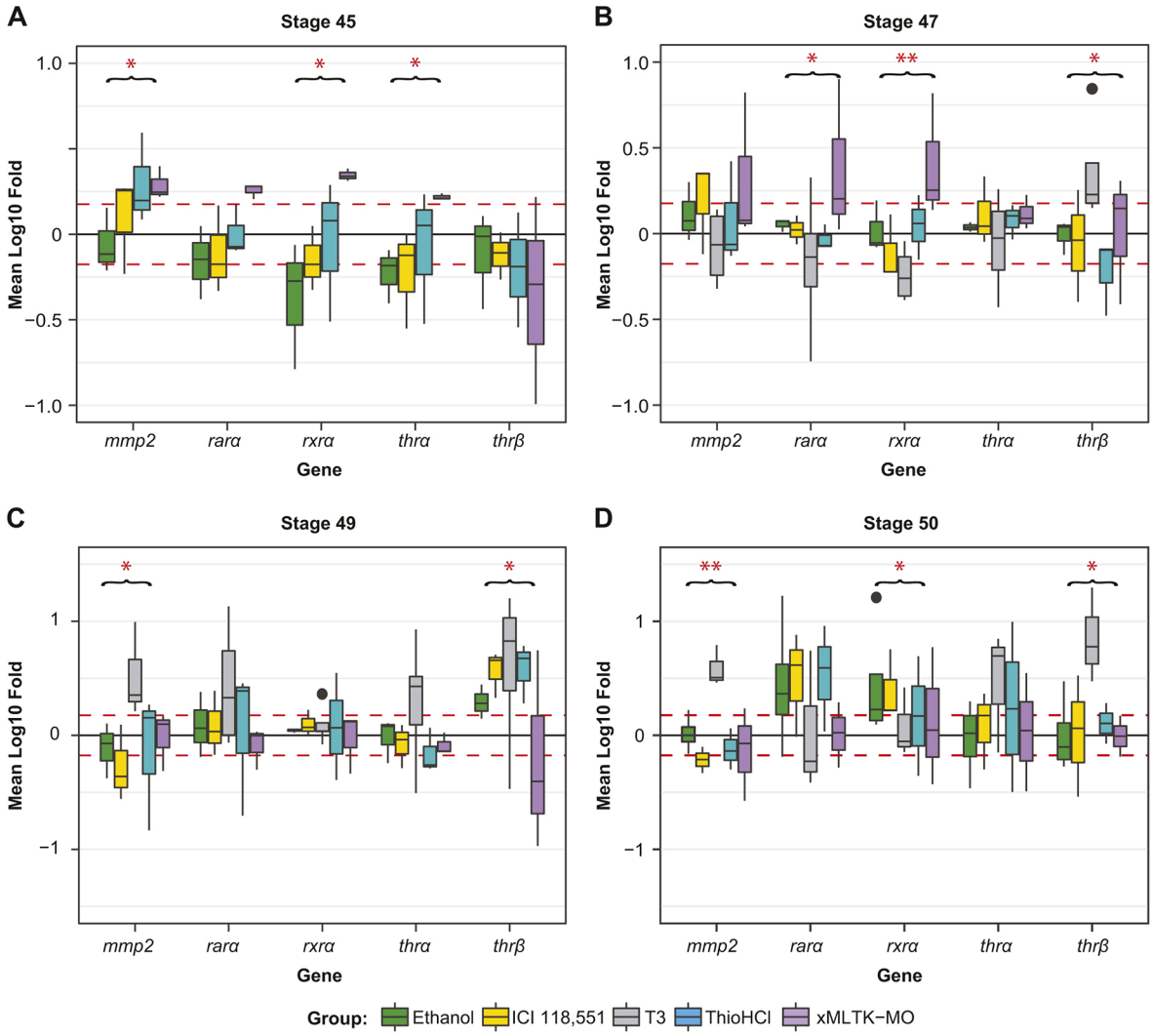

Fig. 4. Candidate gene expression profiles of tadpoles experiencing adaptive tissue craniofacial remodeling are not consistent with precocious metamorphosis. Expression profiles for *mmp2*, *rarα*, *rxrα*, *thrα* and *thrβ* were analyzed at NF stages 45, 47, 49 and 50 in T3-, thioridazine-, ethanol-, ICI 118,551- and xMLTK-MO-treated tadpoles. The T3-treated group serves as a positive control for mild thyroid hormone induction of the TH pathway for NF stages 47+. Upregulated expression of *mmp2*, *thrα* and *thrβ* is indicative of thyroid hormone pathway induction. Upregulated expression of *rxrα* and *rarα* is indicative of endocrine hormone pathway induction. Mean $\log_{10}$ fold candidate gene expression is relative to the wild-type control group (control $\log_{10}$ fold change=0); mean gene expression levels for controls and experimental tadpoles were first normalized to the eukaryotic elongation factor 1a (*eef1a*) gene. Box and whisker plots: median values (middle bars) ± a quartile (boxes); whiskers indicate 1st and 4th quartile; any outliers are >1.5× the interquartile ranges. The red dashed line indicates a conservative biological significance threshold (1.5× fold change). *N*=3-5 biological replicates, *n*=10 tadpoles per group per stage. **P*<0.05, ***P*<0.001 (Kruskal-Wallis). Total n of 50 for controls, 30 for ethanol, 50 for ICI 118,551, 30 for T3, 50 for thioridazine and 30 for xMLTK-MO.

craniofacial tissue could later be studied via RT-qPCR in other experimental groups.

We found 101 differentially expressed genes between control and thioridazine-treated samples at NF stages 45 and 135 at NF stage 47 (Tables S1, S2). We then performed GO pathway enrichment analysis on the significant gene lists by converting the *X. laevis* gene symbols to *Xenopus tropicalis* gene symbols (Table 2, Table 3). When we examined the list of differentially expressed genes, we identified factors that correlated with upregulation (in the thioridazine tadpoles) of endocrine hormone pathways, such as gonadotropin-releasing hormone and prolactin hormone signaling.

The RNA-seq experiment specifically revealed upregulation of the protein-coding sequence for a prolactin 2 protein (prolactin.2.S) (Tables 2 and 3). From previous studies in *Xenopus* and other animals, we know that prolactin signaling can induce tissue remodeling responses in various tissues (Huang and Brown, 2000; Huang et al., 2009; Jung et al., 2004; Parhar, 2003). Thus, we generated qPCR primers specific to the *prolactin.2.S* sequence to further investigate this hormone in our treated tadpoles with craniofacial defects. We also generated qPCR primers for the prolactin receptor gene after confirming that the prolactin receptor-binding region was conserved among *prolactin.1* and *prolactin.2* in *X. laevis*. With RT-qPCR, we examined the expression of the *prolactin.2.S* and prolactin receptor gene in the brain tissue of thioridazine-, ethanol- and ICI 118,551-treated tadpoles at NF stages 45 and 47 (Fig. S6A,B). Thioridazine-treated tadpoles exhibited a threefold increase in *prolactin.2.S* at NF stages 45 and a fivefold increase at stage 47, with no change in the expression of prolactin receptor at either stage (Fig. S6). Thus, the RNA-seq hit for this prolactin gene has been affirmed.

Prolactin gene expression has been shown to be negatively regulated by dopamine signaling in several animals (Fitzgerald and

Development (2019) 146, dev175893. doi:10.1242/dev.175893

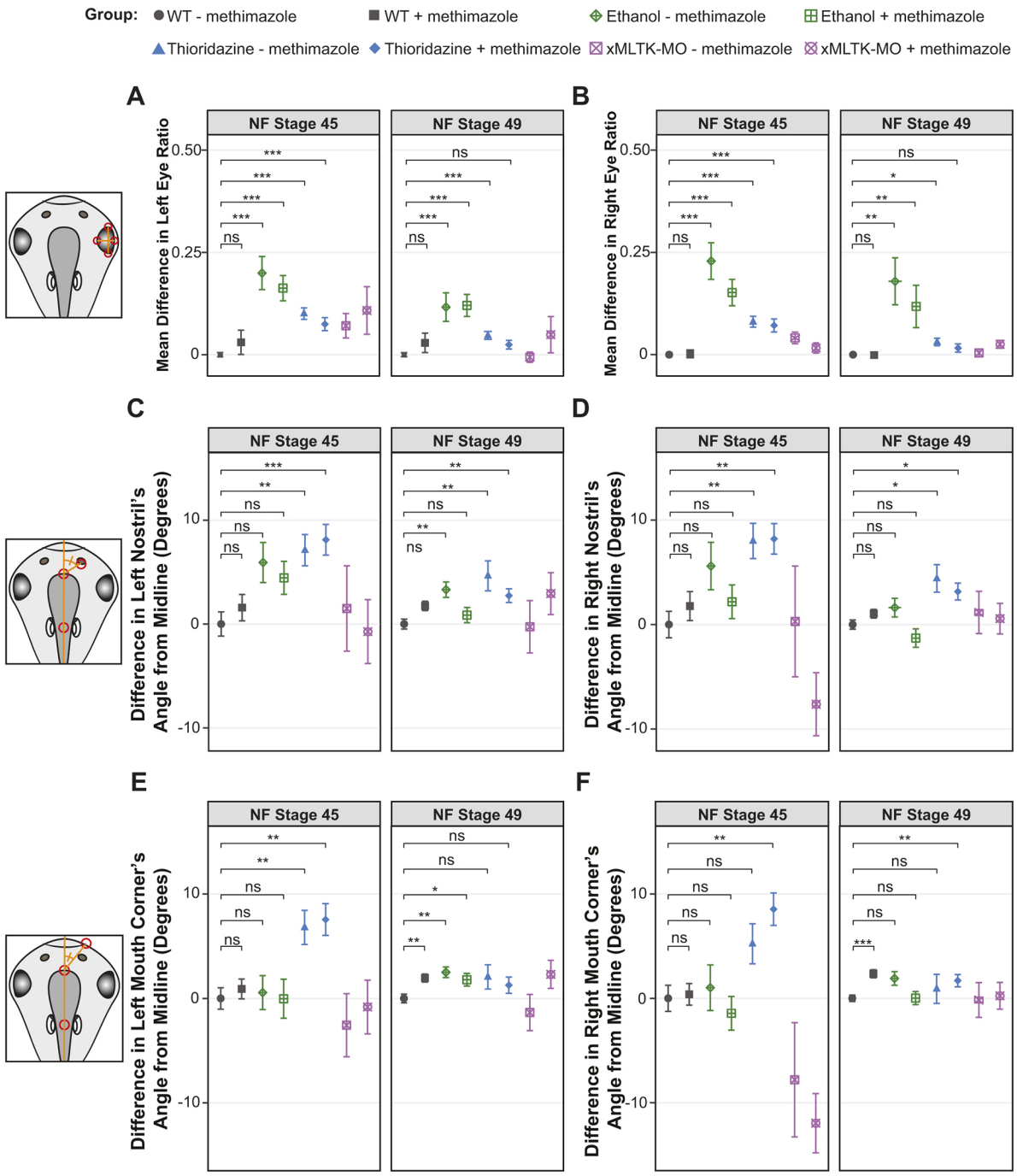

Fig. 5. Thyroid hormone inhibition does not block normalization of abnormal craniofacial morphologies in ethanol-, thioridazine- or xMLTK-MO-treated tadpoles. Morphological metrics (e.g. eye ratio, nostril-midline angle and mouth corner-midline angle) were quantified at NF stages 45 and 49 for wild-type control, ethanol-, thioridazine- and xMLTK-MO-treated tadpoles that were either left in untreated media or exposed to methimazole. Thus, the eight groups are designated wild type±methimazole, ethanol±methimazole, thioridazine±methimazole and xMLTK-MO±methimazole. Measurements are presented as the mean difference between the experimental and control value±s.e.m. For wild-type control, ethanol and thioridazine: *N*=3 biological replicates, *n*=6-18 tadpoles, for a total *n* of 29-48 per group/stage. Total *n* of 47 for wild type±methimazole, 30 for ethanol±methimazole, 35 for thioridazine±methimazole and 13 xMLTK-MO±methimazole. Two-tailed Mann-Witney U test applied to all but xMLTK-MO groups due to the total *n*<25 for each xMLTK-MO group, which is below our set value for adequate statistical power. ns=*P*>0.05, *P<0.05, **P<0.01, ***P<0.001 after Bonferroni adjustment.

Dinan, 2008; Freeman et al., 2000; Treier and Rosenfeld, 1996). Therefore, we deemed it necessary to investigate the effect that increased dopamine signaling and subsequent downregulation of prolactin has on the correction of thioridazine-induced craniofacial defects in *X. laevis*. For this, we exposed control and thioridazine-treated tadpoles to a dopamine signaling agonist, pergolide mesylate (PM), during the stages where we previously observed the correction of craniofacial malformations (NF stages 45-49). We found that the +PM thioridazine-treated group was still able to correct abnormal eye shapes (Fig. 6). Thus, dopamine and prolactin

Development (2019) 146, dev175893. doi:10.1242/dev.175893

Table 2. Gene ontology pathway analysis based on differentially expressed genes between control and thioridazine-treated tadpole head tissue samples at NF stage 45

Number of genes	Pathway
3	Gonadotropin-releasing hormone receptor pathway (P06664)
2	Angiogenesis (P00005)
2	Huntington disease (P00029)
2	VEGF signaling pathway (P00056)
2	*De novo* pyrimidine deoxyribonucleotide and purine biosynthesis (P02739, P02738)
2	Muscarinic acetylcholine receptor 1 and 3+2 and 4 signaling pathway (P00042, P00043)
2	Metabotropic glutamate receptor group II and III pathway (P00040, P00039)
1	p38 MAPK pathway (P05918)
1	Inflammation mediated by chemokine and cytokine signaling pathway (P00031)
1	Endothelin signaling pathway (P00019)
1	Nicotinic acetylcholine receptor signaling pathway (P00044)
1	B cell activation (P00010)
1	CCKR signaling map (P06959)
1	Tetrahydrofolate biosynthesis (P02742)
1	p53 pathway (P00059)
1	Wnt signaling pathway (P00057)
1	Synaptic vesicle trafficking (P05734)
1	T cell activation (P00053)

Total number of differential genes: 101.
Number of differential genes with *X. tropicalis* homologues for GO analysis: 26.
Total pathway hits: 18.

signaling do not appear to be necessary for the remodeling of abnormal eye tissue. However, PM exposure did block the ability of thioridazine-treated tadpoles to correct abnormal angles between the nostrils and the midline. Furthermore, PM exposure significantly affected the angles between the midline and the nostrils of tadpoles that originally had wild-type craniofacial phenotypes at NF stage 45, by NF stage 49 (MWU Test, $P<0.001$) (Fig. 6, Fig S7). A similar but milder effect was also seen with the angle between the midline and the edges of the mouth: at stage 49, both +PM groups had slightly more obtuse mean angle values than −PM controls. Thus, increasing dopamine signaling via PM exposure disrupts the normal maintenance of overall craniofacial morphology in wild-type animals, as well as the correction of abnormal craniofacial morphology in animals with thioridazine-induced craniofacial defects.

TH-independent upregulation of *mmp1* and *mmp13* occurs in malformed craniofacial tissue undergoing adaptive correction

Given that matrix metalloproteinases (MMPs) are key factors for tissue remodeling in animals (Jabłońska-Trypuć et al., 2016) and that prolactin signaling regulates *mmp1* and *mmp13* expression in *X. laevis* (Jung et al., 2004), we chose to examine the expression of these genes at NF stages 47 and 49 in xMLTK-MO-, ethanol-, thioridazine- and ICI 118, 551-treated craniofacial tissue. We determined that *mmp13* was significantly upregulated in xMLTK-MO-treated craniofacial tissues at NF stage 47 (Dunn's test, d.f.=4, $P<0.05$) (Fig. 7A). Although both *mmp1* and *mmp13* were upregulated in ethanol-, thioridazine- and ICI 118,551-treated tadpoles at NF stage 49 (Dunn's test, d.f.=4, $P<0.05$) (Fig. 7B). These data correlate with there being a tissue remodeling response occurring in the craniofacial tissues of these tadpoles that involves various MMPs.

Table 3. Gene ontology pathway analysis based on differentially expressed genes between control and thioridazine-treated tadpole head tissue samples at NF stage 47

Number of genes	Pathway
8	Heterotrimeric G-protein signaling pathway (P00028, P00026, P00027)
5	Wnt signaling pathway (P00057)
4	5-HT type receptor-mediated signaling pathway (P04375, P04374, P04373, P04376)
4	Inflammation mediated by chemokine and cytokine signaling pathway (P00031)
4	Metabotropic glutamate receptor group II and III pathway (P00040, P00039)
4	p53 pathway (P00059, P04398, P04397, P04392)
3	Angiotensin II-stimulated signaling through G proteins and β-arrestin (P05911)
3	Apoptosis signaling pathway (P00006)
3	β-Adrenergic receptor signaling pathway (P04379, P04378)
3	Gonadotropin-releasing hormone receptor pathway (P06664)
3	Muscarinic acetylcholine receptor 1 and 3+2 and 4 signaling pathway (P00042, P00043)
3	Opioid pathway (P05916, P05915, P05917)
2	CCKR signaling map (P06959)
2	Histamine H1 and H2 receptor-mediated signaling pathway (P04385,P04386)
2	PI3 kinase pathway (P00048)
1	Adenine and hypoxanthine salvage pathway (P02723)
1	Adrenaline and noradrenaline biosynthesis (P00001)
1	Angiogenesis (P00005)
1	Cortocotropin-releasing factor receptor signaling pathway (P04380)
1	Cytoskeletal regulation by Rho GTPase (P00016)
1	Endogenous cannabinoid signaling (P05730)
1	Endothelin signaling pathway (P00019)
1	Enkephalin release (P05913)
1	FAS signaling pathway (P00020)
1	GABA-B receptor II signaling (P05731)
1	Huntington disease (P00029)
1	Ionotropic glutamate receptor pathway (P00037)
1	Isoleucine biosynthesis (P02748)
1	Nicotine degradation (P05914)
1	Nicotinic acetylcholine receptor signaling pathway (P00044)
1	Oxytocin receptor-mediated signaling pathway (P04391)
1	p38 MAPK pathway (P05918)
1	PDGF signaling pathway (P00047)
1	Plasminogen activating cascade (P00050)
1	Purine metabolism (P02769)
1	Tetrahydrofolate biosynthesis (P02742)
1	Thyrotropin-releasing hormone receptor signaling pathway (P04394)
1	VEGF signaling pathway (P00056)
1	Vitamin D metabolism and pathway (P04396)

Total number of differential genes: 135.
Number of differential genes with *X. tropicalis* homologues for GO analysis: 77.
Total pathway hits: 39.

DISCUSSION

This work demonstrates that *X. laevis* pre-metamorphic tadpoles are capable of correcting abnormal craniofacial phenotypes resulting from several different embryonic perturbations, in addition to the previously noted knockdown of H^+-V-ATPase (Vandenberg et al., 2012). These additional examples of perturbation that result in self-correcting abnormalities include ethanol exposure, thioridazine exposure and morpholino-based knockdown of xMLTK (Fig. 1). Furthermore, in accordance with previous studies on the morphological changes that occur in craniofacial cartilaginous features (Rose, 2014; Rose et al., 2015), we found that, as tadpoles

Development (2019) 146, dev175893. doi:10.1242/dev.175893

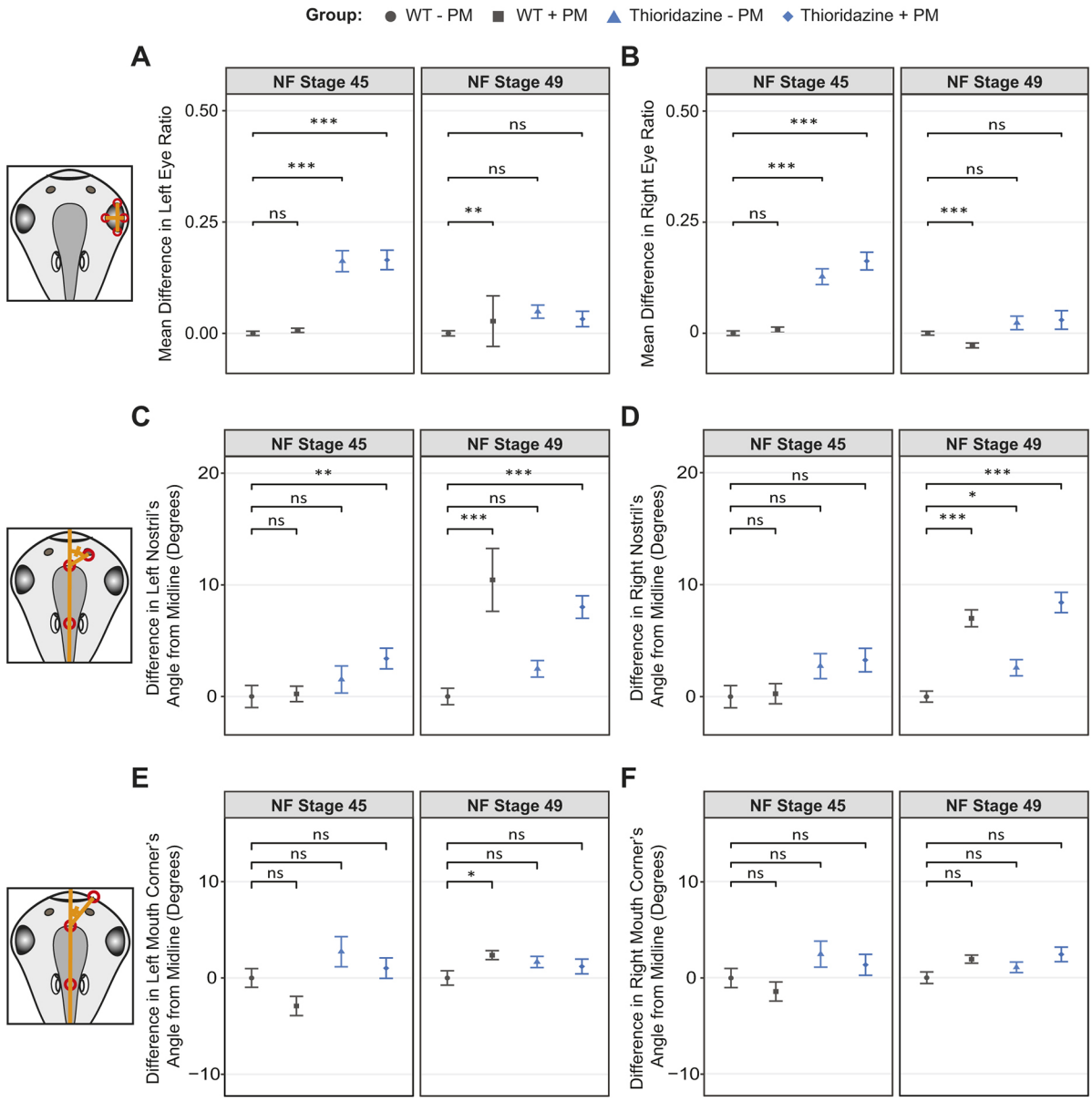

Fig. 6. Increased dopamine signaling hinders normalization of abnormal craniofacial morphologies in thioridazine-treated tadpoles. Morphological metrics (e.g. eye ratio, nostril-midline angle and mouth corner-midline angle) were quantified at NF stages 45 and 49 for wild-type control and thioridazine-treated tadpoles that were either left in untreated media or exposed to pergolide mesylate (PM). Thus, the four groups are designated wild type±PM and thioridazine±PM. Measurements are presented as the mean difference between the experimental and control value±s.e.m. Two-tailed Mann-Witney U test: ns=P>0.05, *P<0.05, **P<0.01, ***P<0.001 after Bonferroni adjustment. N=3 biological replicates, n=14-18 tadpoles per group per stage. Total n of 47 for wild type−PM, 48 for wild type+PM, 48 for thioridazine−PM and 45 for thioridazine+PM.

progress from early to late pre-metamorphic stages, there is a decrease in the within-group variance in morphological measurements among control and experimental tadpole groups. Therefore, it seems that there is an innate and adaptive mechanism present in all *X. laevis* larvae with the potential to recognize and address certain malformed or misaligned craniofacial features (Fig. 8).

We know, however, that this adaptive mechanism is not infallible because we have also shown that there are some perturbations that result in permanent craniofacial defects (Fig. 1). For example, in the case of ICI 118,551 exposure, we found that the larvae were unable to correct absent cartilaginous features. Thus, craniofacial cartilage structures cannot be formed *de novo* at these life stages, similar to tail regeneration in pre-metamorphic tadpoles (Beck et al., 2006; Li et al., 2016). This suggests that the self-correction of abnormal craniofacial morphology requires significant tissue remodeling of existing structures.

As thyroid hormone (TH) signaling mediates craniofacial cartilage and central nervous system remodeling during metamorphosis (Buchholz et al., 2006; Das et al., 2006; Shi et al., 1998; Kerney et al., 2012), we examined whether the tissue remodeling observed in our pre-metamorphic tadpoles could be a mild form of precocious metamorphosis. Ultimately, our TH-dependent gene expression profile analysis and pharmacological inhibition of TH production in these tadpoles revealed that the adaptive craniofacial tissue remodeling observed is not a form of precocious metamorphosis. However, we did see increased expression of *rxrα* in tadpoles with self-correcting craniofacial deformities. This increase in nuclear

Development (2019) 146, dev175893. doi:10.1242/dev.175893

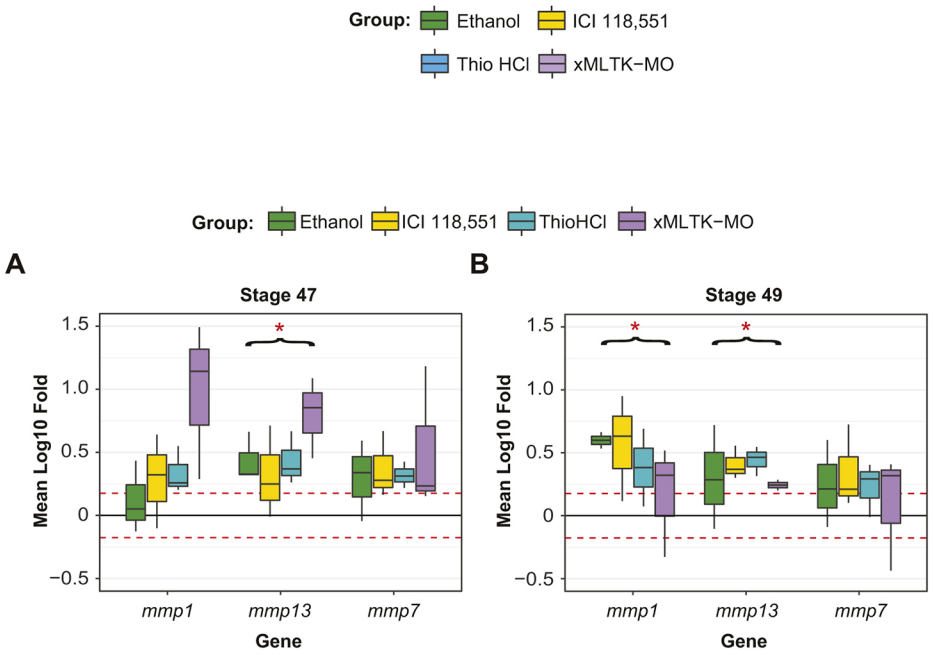

Fig. 7. Differential gene expression of *mmp1*, *mmp13* and *mmp7* in control, ethanol-, thioridazine-, ICI 118,551- and xMLTK-MO-treated tadpoles detected through RT-qPCR. Expression profiles for *mmp7*, *mmp1* and *mmp13* were analyzed at NF stages 47 and 49 in ethanol-, ICI 118,551-, thioridazine- and xMLTK-MO-treated tadpoles. Upregulated expression of Mmp genes is indicative of tissue remodeling pathway induction. Mean $\log_{10}$ fold candidate gene expression is relative to the wild-type control group (control $\log_{10}$ fold change=0); mean gene expression levels for controls and experimental tadpoles were first normalized to the eukaryotic elongation factor 1a (*eef1a*) gene. Box and whisker plots: median values (middle bars) ± a quartile (boxes); whiskers indicate 1st and 4th quartile; any outliers are >1.5× the interquartile ranges. The red dashed line indicates a conservative biological significance threshold (1.5× fold change). *N*=3 biological replicates, *n*=10 tadpoles per group per stage. **P*<0.05 (Kruskal-Wallis U test).

receptors is suggestive of increased nuclear receptor signaling, and nuclear receptor-dependent gene regulation is commonly associated with endocrine hormone signaling and the induction of tissue remodeling events (Escriva et al., 2006; Evans and Mangelsdorf, 2014; Laudet, 2011). Thus, alternate endocrine hormone signaling is likely to be playing a crucial role in the correction abnormal craniofacial morphology in pre-metamorphic tissues.

By pursuing an RNA-seq based approach to monitor gene expression changes in pre-metamorphic thioridazine-treated tadpoles with correctable craniofacial malformations, we identified prolactin signaling as the potential pathway used to direct the craniofacial defect self-correction response (Tables 2 and 3). Although thioridazine is a dopamine-receptor antagonist that causes increased prolactin expression, our work (K.P. and K.A.M., unpublished) and previous work (Huang and Brown, 2000) confirmed that increased prolactin signaling during development alone does not cause evident craniofacial defects; the main effect of prolactin overexpression in *X. laevis* embryos and tadpoles is the retention of their tail into adulthood (Huang and Brown, 2000). Interestingly, prolactin signaling has been previously shown to regulate *mmp1* and *mmp13* expression in *Xenopus* cell cultures in a TH-independent manner (Jung et al., 2004) and these Mmp genes are also upregulated in tadpoles with self-correcting craniofacial defects. Thus, it is possible that prolactin signaling is crucial to the remodeling of cartilaginous tissue within the craniofacial region of these pre-metamorphic animals. This is supported by the fact that increased dopamine signaling, which would subsequently decrease prolactin expression and signaling, disrupts the maintenance of normal craniofacial morphology and correction of abnormal craniofacial morphology in pre-metamorphic *X. laevis* tadpoles (Fig. 6).

Although investigating how malformed craniofacial tissues are naturally corrected in *X. laevis* tadpoles has led us to valuable insights regarding the remodeling of malformed cartilage and eye tissue, there is much more that needs to be deciphered about this process. For example, it would be beneficial to determine to what extent developmental malformities of muscle and brain tissue can be remodeled in *X. laevis* pre-metamorphic tadpoles. Additionally, it is well known that tissue remodeling often involves coordinated cell proliferation, apoptosis, migration and differentiation (Bosurgi et al., 2017; Eom and Parichy, 2017; Lorda-Diez et al., 2015; Pellettieri et al., 2010; Shi et al., 2008). Thus, it would be worthwhile to track and study the cell behaviors responsible for the alteration of abnormal tissue and organ morphology in *X. laevis* larvae. This includes cellular production and release of MMPs into the extracellular matrix (ECM), which may be crucial for ECM remodeling and cell movement.

Finally, we must continue to investigate the impact that various teratogens and developmental perturbations have on cellular mechanisms that are crucial for craniofacial development and morphological regulation in these animals, as there are likely to be distinct regulatory mechanisms involved in monitoring and maintaining the morphology. This will allow us to develop a more precise model for the molecular-, cellular- and tissue-level mechanisms behind the detection and correction of craniofacial defects in *Xenopus laevis* tadpoles. These discoveries ultimately hold great potential for inspiring and guiding novel tissue-remodeling studies, focused on better understanding the mechanisms responsible for maintaining and altering tissue morphology in vertebrate animals.

MATERIALS AND METHODS

Embryo culturing and tadpole rearing

All experiments using *Xenopus laevis* were conducted in accordance with the guide for Care and Use of Laboratory Animals and were approved by the Institutional Animal Care and Use Committee at Tufts University. Embryo culturing was carried out as previously described (Caine and McLaughlin, 2013). Embryos and tadpoles were reared in 0.1× Marc's Modified Ringer's solution [MMR, 10 mM NaCl, 0.2 mM KCl, 0.1 mM CaCl, 0.2 mM $MgCl_2$, 0.5 MM HEPES, 1 µM EDTA (pH 7.5)] at 14-23°C. The 0.1× MMR rearing media was refreshed at least three times a week. Feeding-stage tadpoles were fed Sera Micron powdered growth food three times a week. Embryos and tadpoles were staged based on Nieuwkoop and Faber (1994).

Microinjections and pharmacological exposures

xMLTK morpholino microinjections were performed at Nieuwkoop and Faber (NF) stage 3, into one of two dorsal blastomeres to primarily restrict the effect of the morpholino to half of the head. Morpholino design and purchasing followed previous work by Suzuki et al. with the xMLTK-MO

Development (2019) 146, dev175893. doi:10.1242/dev.175893

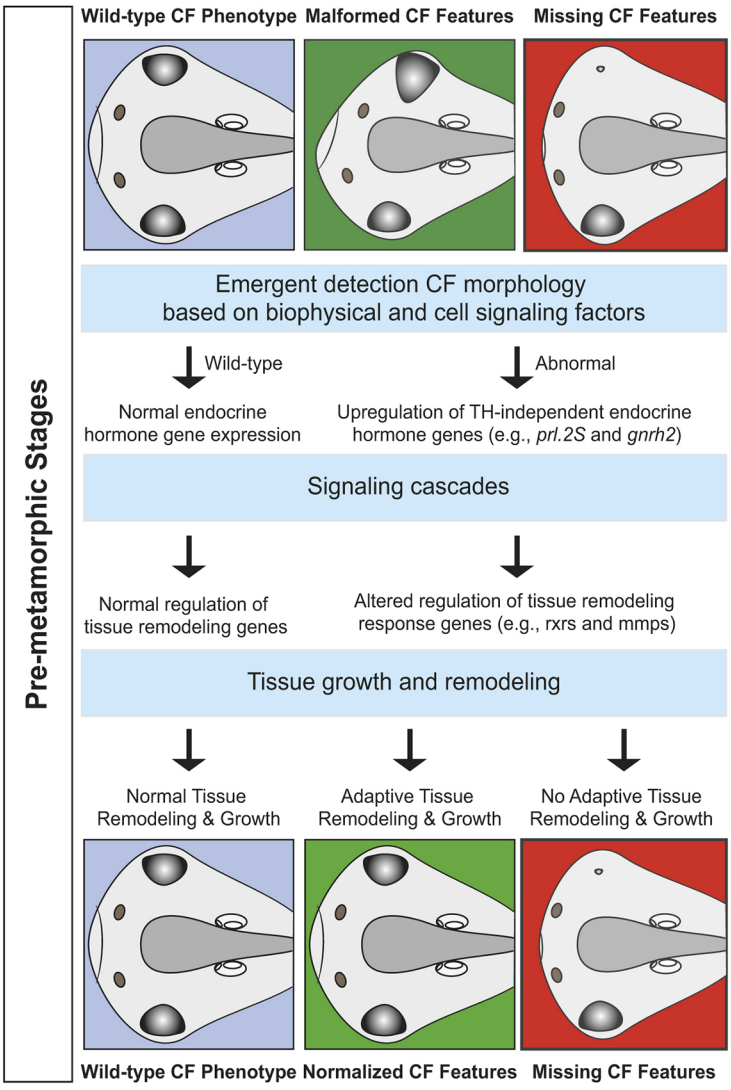

Fig. 8. Model for the adaptive TH-independent tissue remodeling response seen in tadpoles with self-correcting malformed craniofacial features. In both wild-type control and abnormal tadpoles, craniofacial morphology is monitored and adaptively regulated through innate growth and tissue remodeling mechanisms. Tadpoles with abnormal craniofacial morphology shown to self-correct prior to metamorphosis (middle) trigger a more-robust tissue remodeling and growth phase through the upregulation of endocrine hormone genes (e.g. *prolactin.2.S*) relative to controls. Tadpoles with abnormal craniofacial morphology that do not self-correct prior to metamorphosis (right) are either unable to increase endocrine hormone signaling or have missing craniofacial features.

(Suzuki et al., 2012). Pharmacological exposures to induce craniofacial defects were conducted on neurula stage embryos (NF stage 14-26) that had been reared at 14°C prior to exposure. During the exposure windows, experimental and controls embryos were kept at 18°C; after the exposure they were returned to 14°C until they reached feeding-tadpole stages. Pharmacological treatments included: 1.5% ethanol, 90 µM thioridazine (thioridazine-HCl, Tocris), and 200 µM ICI 118,551 (Tocris). Plate densities during exposures were kept at 50 embryos per 10 ml of media. To generate positive controls for precocious metamorphosis or prevent thyroid hormone production, we applied either a 0.5 nM thyroid hormone (Tocris) or 100 mM methimazole treatment to tadpoles from NF stage 45 to 50, respectively. Prolactin inhibition was carried out through 5 µm pergolide mesylate (Sigma) exposures continuously from stages 45 to 49.

Landmark-based geometric morphometric analysis

Live specimens were temporarily immobilized for imaging with a mild tricaine exposure, then dorsal view photos for morphological analysis were taken on a Nikon SMZ1500 dissection microscope with a Spot Insight Color digital camera and Spot Image Solutions software. Landmarks were applied to the images with (StereoMorph R package). The primary landmarks used for GMA were: (1) right nostril; (2) right mouth corner; (3) medial edge of right eye; (4) lateral edge of right eye; (5) anterior edge of right eye; (6) posterior edge of left eye; (7) right otolith; (8) left otolith; (9) medial edge of left eye; (10) lateral edge of left eye; (11) anterior edge of left eye; (12) posterior edge of right eye; (13) left mouth corner; (14) left nostril; (15) anterior end of brain; and (16) midpoint between otoliths. Relative angles and distances between landmarks were calculated using a custom R script, while morphometric analyses were carried out using MorphoJ (Klingenberg, 2011).

Whole-mount *in situ* hybridization and Alcian Blue staining

Euthanized tadpoles were fixed in 1× MEMFA [0.1 M MOPS (pH 7.4), 2 mM EGTA, 1 mM $MgSO_4$, 3.7% formaldehyde], washed with 1× phosphate-buffered saline (PBS), dehydrated in methanol, bleached overnight at room temperature with a 9% hydrogen peroxide solution under a constant light source, transitioned to 100% methanol and stored at −20°C until used for whole-mount *in situ* hybridization or Alcian Blue staining. *In situ* hybridization was performed as described previously (Caine and McLaughlin, 2013), using a *sox9* antisense RNA probe (Vandenberg et al., 2011). Alcian Blue staining was carried out over 2 days at 20-37°C, afterwards specimens were placed in a 20% glycerol clearing solution. We characterized changes in cartilage tissue morphology during self-correction of abnormal craniofacial phenotypes by applying Alcian Blue staining and tracking the percent of unperturbed control, thioridazine, ethanol, ICI 118,551 and xMLTK-MO tadpoles with severely malformed, moderately malformed and normal craniofacial cartilage at NF stages 45, 47 and 49; scoring followed a qualitative cartilage morphology scoring key (Fig. S3).

Real-time quantitative PCR (RT-qPCR) and RNA-seq

RNA libraries were generated using the Qiagen RNeasy Mini kit and DNAse treated prior to generating cDNA libraries for either RT-qPCR or RNA-seq. RT-qPCR cDNA libraries were generated with M-MuLV Reverse

Transcriptase (NEB), following the manufacturer's protocol. RT-qPCR reactions were set up using Applied Biosystems SYBR Green Master Mix and run on Applied Biosystems 7300 Real-Time PCR System. See Table S3 for RT-qPCR primer sequences.

RNA-seq cDNA libraries were constructed using the Illumina Truseq RNA Library Preparation Kit v2, following the manufacturer's protocol. We applied Quibit analysis to quantify the RNA-seq cDNA libraries, which were then pooled and run on Illumina Hi-Seq 2500 at the Tufts University Core Facility to generate 100 bp single-end reads. Subsequent reads were trimmed to remove adapter sequences and filtered to remove any low-quality reads with Trimmomatic, then mapped to the *Xenopus laevis* genome v9.1 with HISAT2. Transcript count tables were generated with HTSeq-count and differential gene analysis was carried out using the DESeq2 package in R (Love et al., 2014). To perform gene ontology analysis, *X. laevis* gene hits were BLASTed against the *Xenopus tropicalis* genome and the corresponding *X. tropicalis* gene IDs were applied to PANTHER.

Statistics

To promote suitable statistical power, a minimum total samples size (total n) of 25 tadpoles per control and experimental group was applied; total n is the sum of samples sizes (n) across multiple biological replicates (N). Categorical data across multiple control and experimental groups were statistically analyzed using χ^2 GOF tests, with expected values set to the average control values at a given developmental stage. Quantitative data across multiple control and experimental groups were statistically analyzed using Kruskal-Wallis non-parametric tests. If significance was detected with the Kruskal-Wallis test, a post-hoc Mann-Whitney *U*-test or Dunn's test was applied. Bonferroni *P*-value adjustments were employed to compensate for multiple testing bias. Given that the geometric morphometric data displayed non-normal distributions, standard error bars are presented in these graphs as opposed to confidence intervals.

Acknowledgements

We appreciate the numerous helpful discussions with members of the McLaughlin and Levin labs, as well as many others in the developmental biology field.

Competing interests

The authors declare no competing or financial interests.

Author contributions

Conceptualization: K.P., K.A.M.; Methodology: K.P., K.A.M.; Validation: K.P., K.A.M.; Formal analysis: K.P., B.L., M.D.; Investigation: K.P., B.L., M.D., K.A.M.; Resources: K.A.M.; Data curation: K.P., B.L., M.D.; Writing - original draft: K.P.; Writing - review & editing: K.P., K.A.M.; Visualization: K.P., K.A.M.; Supervision: K.P., K.A.M.; Project administration: K.A.M.; Funding acquisition: K.A.M.

Funding

We appreciatively acknowledge support from an Allen Discovery Center award from The Paul G. Allen Frontiers Group (12171).

Data availability

The raw RNA-seq reads and processed gene transcript counts have been deposited in the GEO repository under accession number GSE128772.

Supplementary information

Supplementary information available online at
http://dev.biologists.org/lookup/doi/10.1242/dev.175893.supplemental

References

Beck, C. W., Christen, B., Barker, D. and Slack, J. M. (2006). Temporal requirement for bone morphogenetic proteins in regeneration of the tail and limb of Xenopus tadpoles. *Mech. Dev.* **123**, 674-688. doi:10.1016/j.mod.2006.07.001

Blanco-Davila, F. (2003). Incidence of cleft lip and palate in the northeast of mexico: a 10-year study. *J. Craniofac. Surg.* **14**, 533-537. doi:10.1097/00001665-200307000-00027

Bosurgi, L., Cao, Y. G., Cabeza-Cabrerizo, M., Tucci, A., Hughes, L. D., Kong, Y., Weinstein, J. S., Licona-Limon, P., Schmid, E. T., Pelorosso, F. et al. (2017). Macrophage function in tissue repair and remodeling requires IL-4 or IL-13 with apoptotic cells. *Science* **356**, 1072-1076. doi:10.1126/science.aai8132

Buchholz, D. R., Paul, B. D., Fu, L. and Shi, Y. B. (2006). Molecular and developmental analyses of thyroid hormone receptor function in Xenopus laevis, the African clawed frog. *Gen. Comp. Endocrinol.* **145**, 1-19. doi:10.1016/j.ygcen.2005.07.009

Bylund, D. B., Eikenberg, D. C., Hieble, J. P., Langer, S. Z., Lefkowitz, R. J., Minneman, K. P., Molinoff, P. B., Ruffolo, R. R. and Trendelenburg, U. (1994). International union of pharmacology nomenclature of adrenoceptors. *Pharmacol. Rev.* **46**, 121-136.

Caine, S. T. and McLaughlin, K. A. (2013). Regeneration of functional pronephric proximal tubules after partial nephrectomy in Xenopus laevis. *Dev. Dyn.* **242**, 219-229. doi:10.1002/dvdy.23916

Das, B., Cai, L., Carter, M. G., Piao, Y.-L., Sharov, A. A., Ko, M. S. H. and Brown, D. D. (2006). Gene expression changes at metamorphosis induced by thyroid hormone in Xenopus laevis tadpoles. *Dev. Biol.* **291**, 342-355. doi:10.1016/j.ydbio.2005.12.032

Degitz, S. J., Holcombe, G. W., Flynn, K. M., Kosian, P. A., Korte, J. J. and Tietge, J. E. (2005). Progress towards development of an amphibian-based thyroid screening assay using Xenopus laevis. organismal and thyroidal responses to the model compounds 6-propylthiouracil, methimazole, and thyroxine. *Toxicol. Sci.* **87**, 353-364. doi:10.1093/toxsci/kfi246

Eom, D. S. and Parichy, D. M. (2017). A macrophage relay for long-distance signaling during postembryonic tissue remodeling. *Science* **355**, 1317-1320. doi:10.1126/science.aal2745

Escriva, H., Bertrand, S., Germain, P., Robinson-Rechavi, M., Umbhauer, M., Cartry, J., Duffraisse, M., Holland, L., Gronemeyer, H. and Laudet, V. (2006). Neofunctionalization in vertebrates: the example of retinoic acid receptors. *PLoS Genet.* **2**, e102. doi:10.1371/journal.pgen.0020102

Evans, R. M. and Mangelsdorf, D. J. (2014). Nuclear receptors, RXR & the big bang. *Cell* **157**, 255-266. doi:10.1016/j.cell.2014.03.012

Fainsod, A. and Kot-Leibovich, H. (2017). Xenopus embryos to study fetal alcohol syndrome, a model for environmental teratogenesis. *Biochem. Cell Biol.* **96**, 77-87. doi:10.1139/bcb-2017-0219

Fitzgerald, P. and Dinan, T. G. (2008). Prolactin and dopamine: what is the connection? a review article. *J. Psychopharmacol.* **22**, 12-19. doi:10.1177/0269216307087148

Freeman, M. E., Kanyicska, B., Lerant, A. and Nagy, G. (2000). Prolactin: structure, function, and regulation of secretion. *Physiol. Rev.* **80**, 1523-1631. doi:10.1152/physrev.2000.80.4.1523

Fujimoto, K., Nakajima, K. and Yaoita, Y. (2007). Expression of matrix metalloproteinase genes in regressing or remodeling organs during amphibian metamorphosis. *Dev. Growth Differ.* **49**, 131-143. doi:10.1111/j.1440-169X.2007.00916.x

Gregg, T., Boyd, D. and Richardson, A. (1994). The incidence of cleft lip and palate in Northern Ireland from 1980-1990. *Br. J. Orthod.* **21**, 387-392. doi:10.1179/bjo.21.4.387

Hornung, M. W., Degitz, S. J., Korte, L. M., Olson, J. M., Kosian, P. A., Linnum, A. L. and Tietge, J. E. (2010). Inhibition of thyroid hormone release from cultured amphibian thyroid glands by methimazole, 6-propylthiouracil, and perchlorate. *Toxicol. Sci.* **118**, 42-51. doi:10.1093/toxsci/kfq166

Huang, H. and Brown, D. D. (2000). Prolactin is not a juvenile hormone in Xenopus laevis metamorphosis. *Proc. Natl Acad. Sci. USA* **97**, 195-199. doi:10.1073/pnas.97.1.195

Huang, X., Hui, M. N. Y., Liu, Y., Yuen, D. S. H., Zhang, Y., Chan, W. Y., Lin, H. R., Cheng, S. H. and Cheng, C. H. K. (2009). Discovery of a novel prolactin in non-mammalian vertebrates: evolutionary perspectives and its involvement in teleost retina development. *PLoS ONE* **4**, e6163. doi:10.1371/journal.pone.0006163

Jabłońska-Trypuć, A., Matejczyk, M. and Rosochacki, S. (2016). Matrix metalloproteinases (MMPs), the main extracellular matrix (ECM) enzymes in collagen degradation, as a target for anticancer drugs. *J. Enzyme Inhib. Med. Chem.* **31**, 177-183. doi:10.3109/14756366.2016.1161620

Jung, J.-C., West-Mays, J. A., Stramer, B. M., Byrne, M. H., Scott, S., Mody, M. K., Sadow, P. M., Krane, S. M. and Fini, M. E. (2004). Activity and expression of Xenopus laevis matrix metalloproteinases: identification of a novel role for the hormone prolactin in regulating collagenolysis in both amphibians and mammals. *J. Cell. Physiol.* **201**, 155-164. doi:10.1002/jcp.20037

Kerney, R. R., Brittain, A. L., Hall, B. K. and Buchholz, D. R. (2012). Cartilage on the move: Cartilage lineage tracing during tadpole metamorphosis. *Dev. Growth Differ.* **54**, 739-752. doi:10.1111/dgd.12002

Kilts, C. D., Knight, D. L., Mailman, R. B., Widerlöv, E. and Breese, G. R. (1984). Effects of thioridazine and its metabolites on dopaminergic function: drug metabolism as a determinant of the antidopaminergic actions of thioridazine. *J. Pharmacol. Exp. Ther.* **231**, 334-342.

Klingenberg, C. P. (2011). MorphoJ: an integrated software package for geometric morphometrics. *Mol. Ecol. Resour.* **11**, 353-357. doi:10.1111/j.1755-0998.2010.02924.x

Kot-Leibovich, H. and Fainsod, A. (2009). Ethanol induces embryonic malformations by competing for retinaldehyde dehydrogenase activity during vertebrate gastrulation. *Dis. Model. Mech.* **2**, 295-305. doi:10.1242/dmm.001420

Laudet, V. (2011). The origins and evolution of vertebrate metamorphosis. *Curr. Biol.* **21**, R726-R737. doi:10.1016/j.cub.2011.07.030

Lee, S. and Privalsky, M. L. (2005). Heterodimers of retinoic acid receptors and thyroid hormone receptors display unique combinatorial regulatory properties. *Mol. Endocrinol.* **19**, 863-878. doi:10.1210/me.2004-0210
Li, D., Li, T., Wang, F., Tian, H. and Samuels, H. H. (2002). Functional evidence for retinoid x receptor (RXR) as a nonsilent partner in the thyroid hormone receptor/RXR heterodimer. *Mol. Cell. Biol.* **22**, 5782-5792. doi:10.1128/MCB.22.16.5782-5792.2002
Li, J., Zhang, S. and Amaya, E. (2016). The cellular and molecular mechanisms of tissue repair and regeneration as revealed by studies in Xenopus. *Regeneration* **3**, 198-208. doi:10.1002/reg2.69
Lorda-Diez, C. I., Garcia-Riart, B., Montero, J. A., Rodriguez-León, J., Garcia-Porrero, J. A. and Hurle, J. M. (2015). Apoptosis during embryonic tissue remodeling is accompanied by cell senescence. *Aging* **7**, 974-985. doi:10.18632/aging.100844
Love, M. I., Huber, W. and Anders, S. (2014). Moderated estimation of fold change and dispersion for RNA-seq data with DESeq2. *Genome Biol.* **15**, 550. doi:10.1186/s13059-014-0550-8
Marrs, J. A., Clendenon, S. G., Ratcliffe, D. R., Fielding, S. M., Liu, Q. and Bosron, W. F. (2010). Zebrafish fetal alcohol syndrome model: effects of ethanol are rescued by retinoic acid supplement. *Alcohol* **44**, 707-715. doi:10.1016/j.alcohol.2009.03.004
Nieuwkoop, P. D. and Faber, E. J. (1994). *Normal Table of Xenopus laevis (daudin)*. New York, NY: Routledge.
Parhar, I. S. (2003). Gonadotropin-releasing hormone receptors: neuroendocrine regulators and neuromodulators. *Fish Physiol. Biochem.* **28**, 13-18. doi:10.1023/B:FISH.0000030462.10997.24
Pellettieri, J., Fitzgerald, P., Watanabe, S., Mancuso, J., Green, D. R. and Alvarado, A. S. (2010). Cell death and tissue remodeling in planarian regeneration. *Dev. Biol.* **338**, 76-85. doi:10.1016/j.ydbio.2009.09.015
Rose, C. S. (2014). The importance of cartilage to amphibian development and evolution. *Int. J. Dev. Biol.* **58**, 917-927. doi:10.1387/ijdb.150053cr
Rose, C. S., Murawinski, D. and Horne, V. (2015). Deconstructing cartilage shape and size into contributions from embryogenesis, metamorphosis, and tadpole and frog growth. *J. Anat.* **226**, 575-595. doi:10.1111/joa.12303
Shi, Y. B., Sachs, L. M., Jones, P., Li, Q. and Ishisuya-Oka, Y. (1998). Thyroid hormone regulation of *Xenopus laevis* metamorphosis: functions of thyroid hormone receptors and roles of extracellular matrix remodeling. *Wound Repair. Regen.* **6**, 314-322. doi:10.1046/j.1524-475X.1998.60407.x
Shi, J., Son, M.-Y., Yamada, S., Szabova, L., Kahan, S., Chrysovergis, K., Wolf, L., Surmak, A. and Holmbeck, K. (2008). Membrane-type MMPs enable extracellular matrix permissiveness and mesenchymal cell proliferation during embryogenesis. *Dev. Biol.* **313**, 196-209. doi:10.1016/j.ydbio.2007.10.017
Simões-Costa, M. and Bronner, M. E. (2015). Establishing neural crest identity: a gene regulatory recipe. *Development* **142**, 242-257. doi:10.1242/dev.105445
Simões-Costa, M., Stone, M. and Bronner, M. E. (2015). Axud1 integrates Wnt signaling and transcriptional inputs to drive neural crest formation. *Dev. Cell* **34**, 544-554. doi:10.1016/j.devcel.2015.06.024
Skeberdis, V. A., Jurevičius, J. and Fischmeister, R. (1997). Pharmacological characterization of the receptors involved in the beta-adrenoceptor-mediated stimulation of the L-type Ca2+ current in frog ventricular myocytes. *Br. J. Pharmacol.* **121**, 1277-1286. doi:10.1038/sj.bjp.0701268
Square, T., Jandzik, D., Cattell, M., Coe, A., Doherty, J. and Medeiros, D. M. (2015). A gene expression map of the larval Xenopus laevis head reveals developmental changes underlying the evolution of new skeletal elements. *Dev. Biol.* **397**, 293-304. doi:10.1016/j.ydbio.2014.10.016
Suzuki, T., Kusakabe, M., Nakayama, K. and Nishida, E. (2012). The protein kinase MLTK regulates chondrogenesis by inducing the transcription factor Sox6. *Development* **139**, 2988-2998. doi:10.1242/dev.078675
Tietge, J. E., Butterworth, B. C., Haselman, J. T., Holcombe, G. W., Hornung, M. W., Korte, J. J., Kosian, P. A., Wolfe, M. and Degitz, S. J. (2010). Early temporal effects of three thyroid hormone synthesis inhibitors in Xenopus laevis. *Aquat. Toxicol.* **98**, 44-50. doi:10.1016/j.aquatox.2010.01.014
Treier, M. and Rosenfeld, M. G. (1996). The hypothalamic-pituitary axis; co-development of two organs. *Curr. Opin. Cell Biol.* **8**, 833-843. doi:10.1016/S0955-0674(96)80085-8
Vandenberg, L. N., Adams, D. S. and Levin, M. (2012). Normalized shape and location of perturbed craniofacial structures in the Xenopus tadpole reveal an innate ability to achieve correct morphology. *Dev. Dyn.* **241**, 863-878. doi:10.1002/dvdy.23770
Vandenberg, L. N., Morrie, R. D. and Adams, D. S. (2011). V-ATPase-dependent ectodermal voltage and pH regionalization are required for craniofacial morphogenesis. *Dev. Dyn.* **240**, 1889-1904. doi:10.1002/dvdy.22685
Veldhoen, N., Propper, C. R. and Helbing, C. C. (2014). Enabling comparative gene expression studies of thyroid hormone action through the development of a flexible real-time quantitative PCR assay for use across multiple anuran indicator and sentinel species. *Aquat. Toxicol.* **148**, 162-173. doi:10.1016/j.aquatox.2014.01.008
Wu, Y., Xu, B. and Koenig, R. J. (2001). Thyroid hormone response element sequence and the recruitment of retinoid X receptors for thyroid hormone responsiveness. *J. Biol. Chem.* **276**, 3929-3936. doi:10.1074/jbc.M006743200
Yelin, R., Schyr, R. B., Kot, H., Zins, S., Frumkin, A., Pillemer, G. and Fainsod, A. (2005). Ethanol exposure affects gene expression in the embryonic organizer and reduces retinoic acid levels. *Dev. Biol.* **279**, 193-204. doi:10.1016/j.ydbio.2004.12.014
Yelin, R., Kot, H., Yelin, D. and Fainsod, A. (2007). Early molecular effects of ethanol during vertebrate embryogenesis. *Differentiation* **75**, 393-403. doi:10.1111/j.1432-0436.2006.00147.x

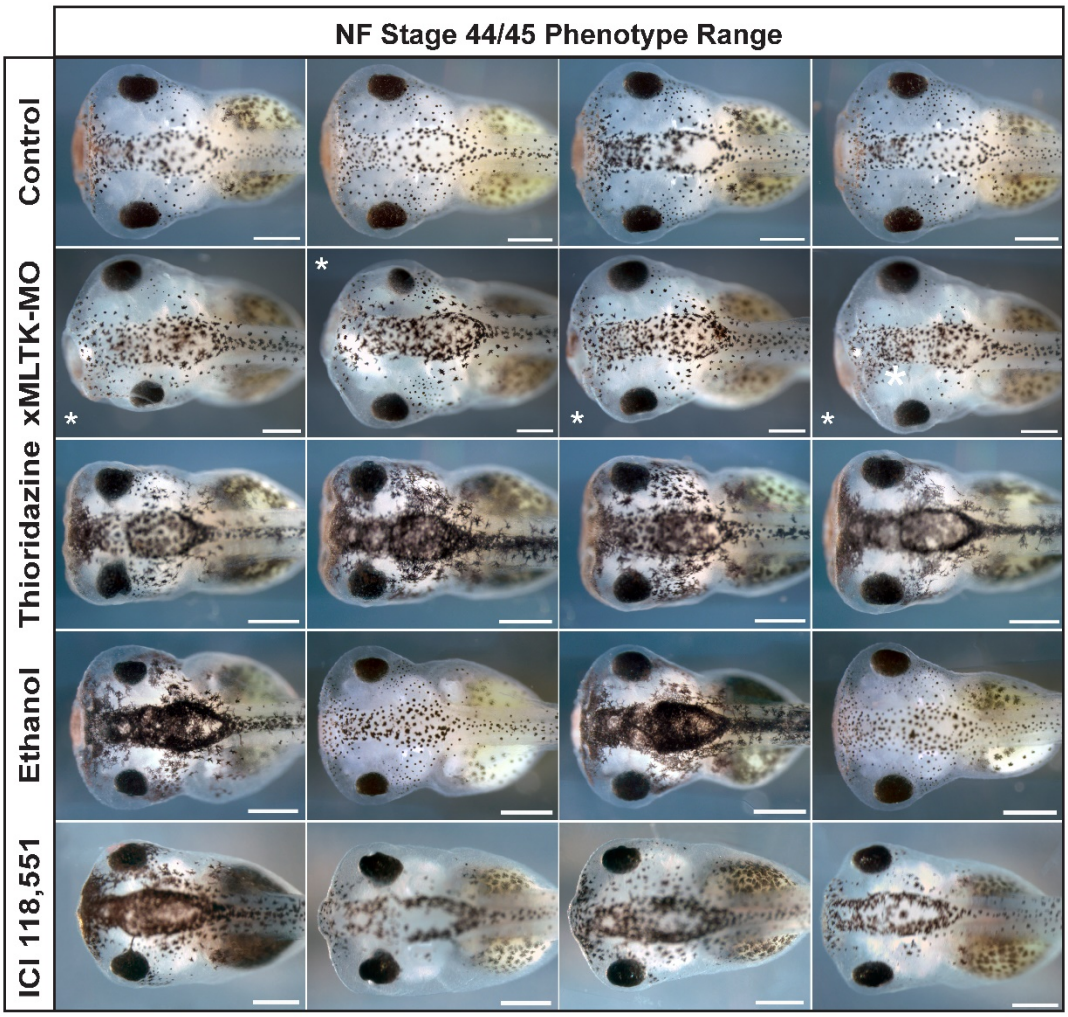

Figure S1. Exposure to xMLTK-MO, thioridazine, ethanol, and ICI 118,551 produces consistent craniofacial phenotypes. Typical range of craniofacial phenotypes observed with these perturbations. For experimental groups the phenotypes are arranged from most abnormal on the left to least abnormal on the right. Morpholino-based knock-down of xMLTK and finite pharmacological (e.g. thioridazine, ethanol, and ICI 118,551) exposures during neurula stages produce abnormal phenotypes with little variation, relative to most teratogens. White asterisks denote the injected side of xMLTK-MO tadpole. Scale bars: 500μm.

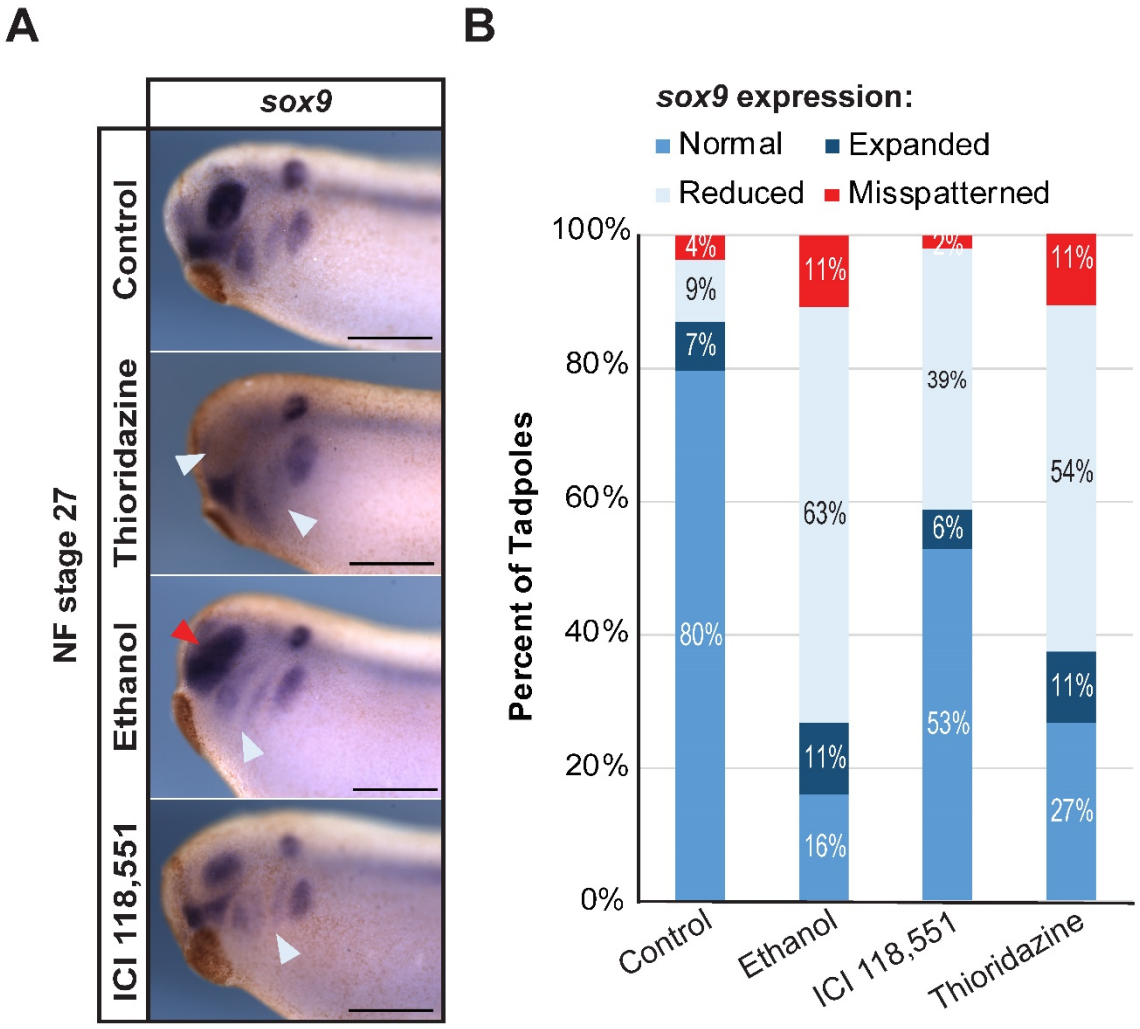

Figure S2. Whole-mount *in situ* hybridization for *sox9* on embryos following exposure to ethanol, ICI 118,551, and thioridazine highlight their effects on neural crest cell localization. A) Representative images showing the range of *sox9* spatial patterning in control and experimental tadpoles. Grey arrowheads point to regions of reduced *sox9* expression, red arrowheads point to mispatterned *sox9* expression. B) Quantification of scored *sox9* phenotypes in control and experimental tadpoles. N = 2, n = 25-29, for a total n of 54 for controls, 56 for ethanol, 51 for ICI 118,551, and 56 for thioridazine. Scale bars: 500μm.

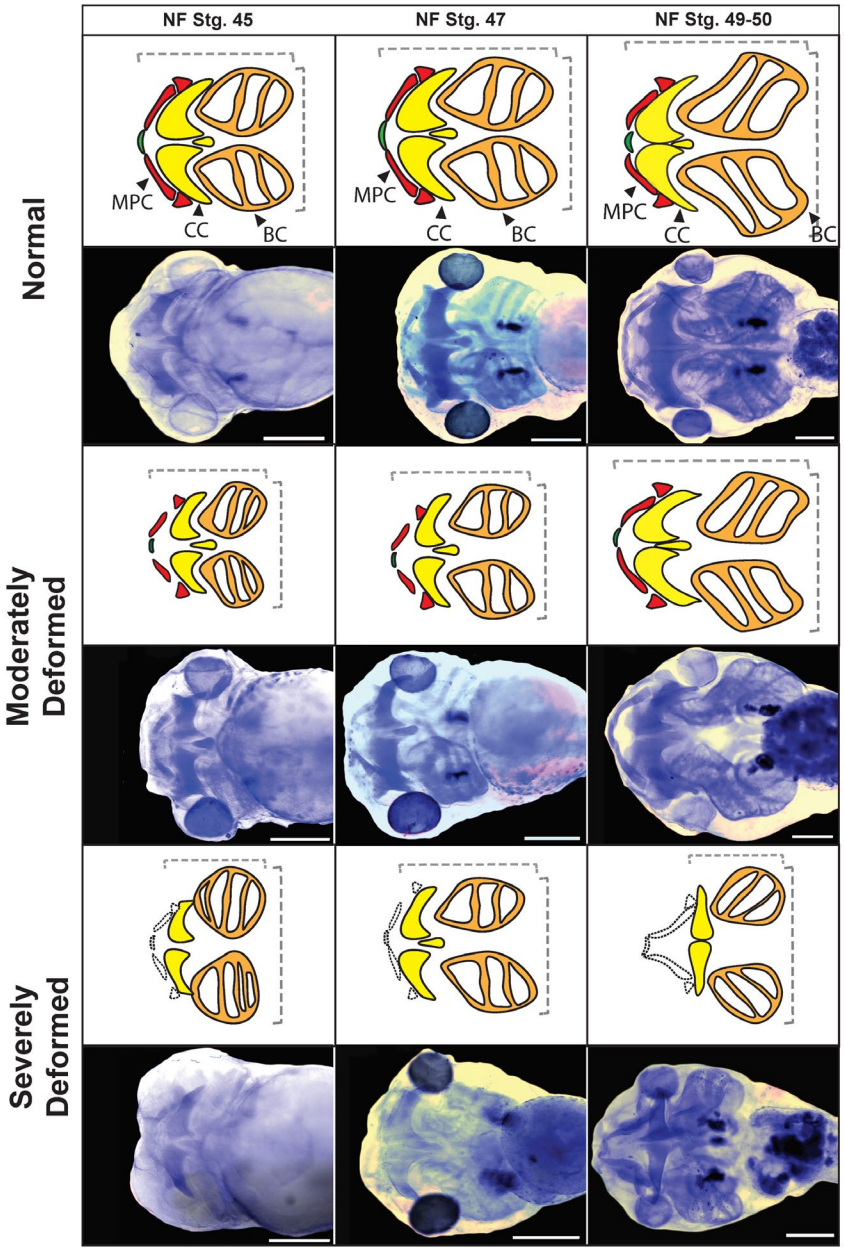

Figure S3. Schematics for cartilage phenotype scoring categories, based on Alcian blue staining. Bleached and Alcian blue stained NF stg. 45-50 specimen, with corresponding WT cartilage schematics. Craniofacial cartilage phenotypes were qualitatively scored as normal, moderate, or severe based on the shape and presence of these major craniofacial cartilaginous features. MPC = Meckel's and Palatoquadrate cartilage, CC = Ceratohyal cartilage, BC = Branchial cartilage. Schematics for severe phenotypes leave uncolored, but outlined, the features commonly missing entirely from the most abnormal specimen. Scale bars: 500μm.

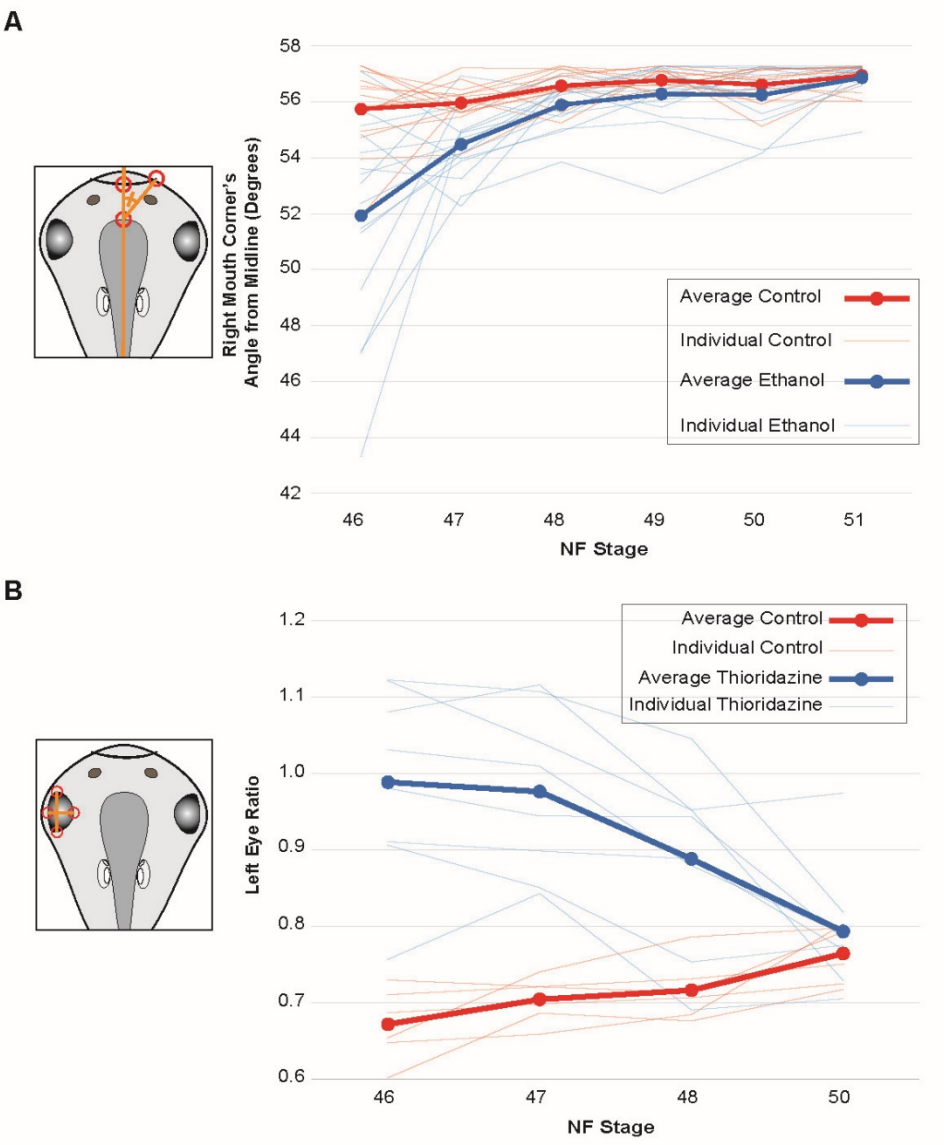

Figure S4. Geometric morphometric analysis in Control, thioridazine, and ethanol tadpoles at pre-metamorphic stages 46-50/51. Morphological metrics (e.g. left eye ratio and right mouth corner-midline angle) were quantified at NF stg 45 through 50 for wild-type control and thioridazine tadpoles. Measurements were taken from Individually tracked tadpoles across several stages, light blue and red lines represent individual experimental tadpoles and control tadpoles, respectively. N = 1 biological replicate, n = 8-15 tadpoles. Opaque blue and red lines represent experimental and control group means, no error bars or statistical tests were applied because data are from a single biological replicate.

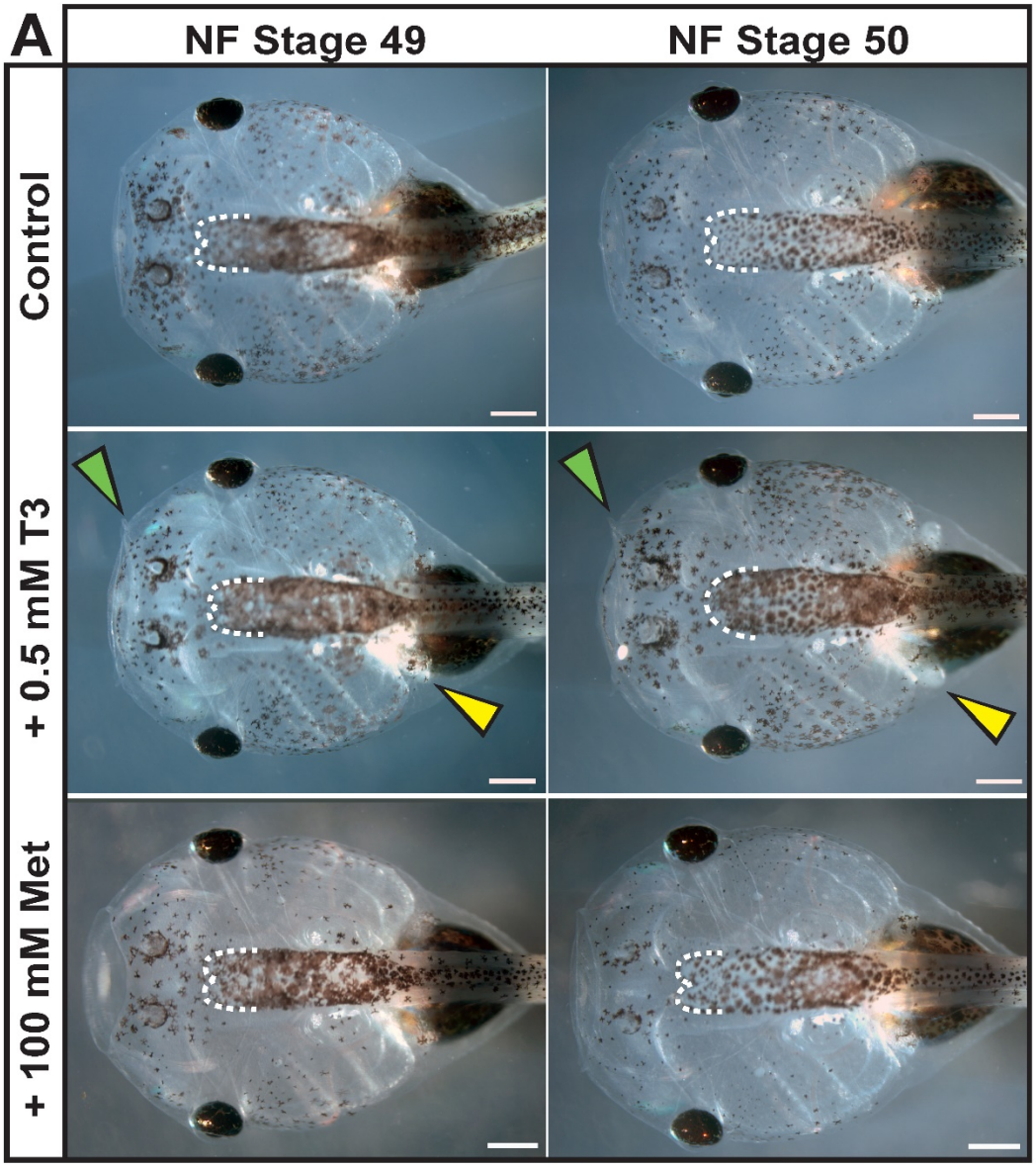

Figure S5. T3 exposure leads to precocious limb bud and barbel growth by NF stages 49 and 50. Representative images of control, +T3 (thyroid hormone), and +Met (methimazole) tadpoles at NF stage 49 and 50. The yellow and green arrow heads point to precocious growth of barbels and limb buds, respectively. The white dashed outline highlights premature or accelerated fusion of the olfactory bulbs in +T3 tadpoles. Scale bars: 500μm.

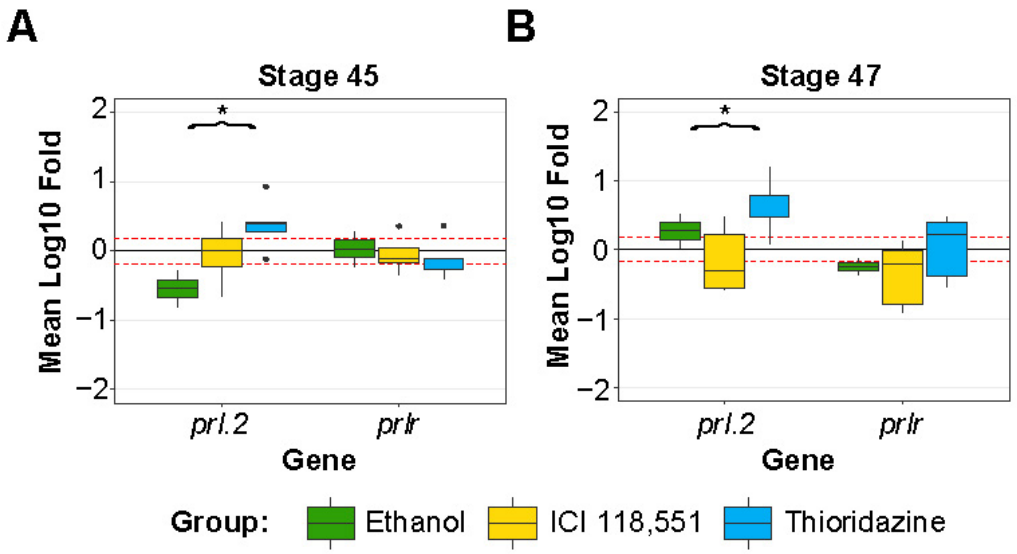

Figure S6. *Prolactin.2.S* is differentially expressed in ethanol and thioridazine tadpoles at NF stage 45 and 47. A,B) Expression of *prolactin.2.S* and *prolactin receptor* was quantified in ethanol, thioridazine, and ICI 118,551 tadpoles at NF stage 45 and 47, respectively. Mean $\log_{10}$ fold candidate gene expression is relative to the WT control group (control $\log_{10}$ fold change = 0); mean gene expression levels for controls and experimental tadpoles were first normalized to the eukaryotic elongation factor 1a (eef1a) gene. The red dashed line denotes a conservative biological significance threshold (1.5x fold change). N = 2-3 biological replicates, n = 10 tadpoles per group per stage. * = KW test, $p < 0.05$.

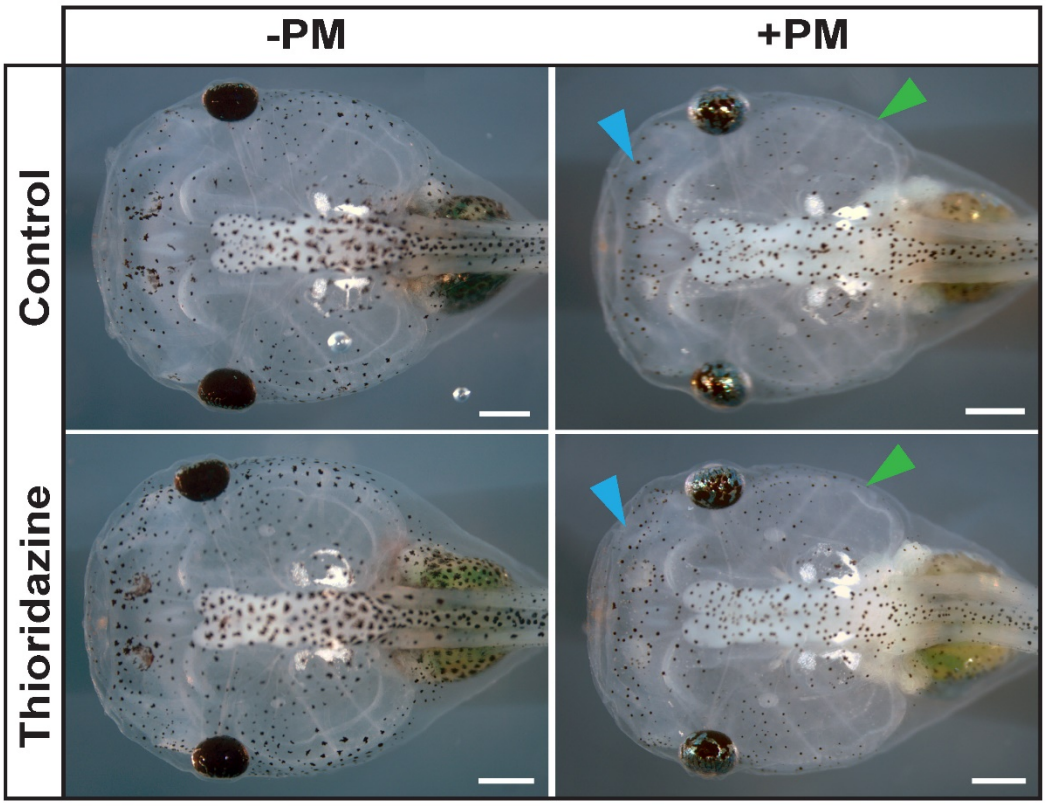

Figure S7. Pergolide mesylate exposure affects the growth and morphology of anterior craniofacial structures and branchial arches. Representative images of wild-type control and thioridazine tadpoles at NF stg 50 that were either left in untreated media (-PM) or exposed to pergolide mesylate (+PM) from NF stg 45 to 50. Pergolide mesylate exposure, reduces branchial arches and anterior CF features, altering the overall head morphology of +PM specimen. Blue arrowhead denotes underdeveloped anterior craniofacial region and green arrowhead denotes reduced branchial arch width, relative to -PM control. Scale bars: 500μm.

Table S1. Differential gene expression in head tissue of tadpoles with thioridazine-induced craniofacial defects at NF stage 45 (Excel file).

Click here to download Table S1

Table S2. Differential gene expression in head tissue of tadpoles with thioridazine-induced craniofacial defects at NF stage 47 (Excel file).

Click here to download Table S2

Table S3. RT-qPCR Primer sequences.

Gene	Gene Symbol	NCBI Gene ID	Forward & Reverse Primers (5'-3')
thrα	*thra.L*	397942	F: AGAAGCTGCCCATGTTCTCT R: ACCTCCGTTCTTAAGCTGCT
thrβ	*thrb.L*	779054	F: CATAGTTAATGCGCCCGAGG R: TGTCACTGCCATCTCACCAT
rxrα	*rxra.L*	378685	F: AAGTACCCATGCATCCCTCC R: GTCTTTGCTATCCCTGCACG
rarα	*rara.L*	399081	F: AGGAGCGAGTTTCTCTGGAC R: GCATCTGAGTGCGGTTTAGG
mmp2	*mmp2.S*	380389	F: ATTCTGGTCGCTCAGATGGC R: GTTTCCGGACAGAAGCCGTA
prl.2	*prl.2.S*	108697263	F: CCGTCAGATTTTAGGGAAAGCC R: CTGGTTCCATGAGCGCAGTA
prlr	*prlr.L*	373618	F: ATATGGGCATTGCTGCACGA R: CCAGGTAGAGACTGCGCGTT
mmp1	*mmp1.S*	495287	F: AAAGAATTGATGCGGCTGTTCA R: GAGCTTGGGGTCCGTCTTATT
mmp13	*mmp13.S*	379564	F: TCCTCCAGACGAGCAGACAT R: CATGGGCAGCAACAAGGAAC
mmp7	*mmp7.S*	379369	F: GCCCCAACCTGAAGATCCTATG R: CCGAGGGGTCTTCATCATCTT